Learning-induced plasticity in vascular properties in the human brain

Avner Fitterman

A Thesis
in
The Department
of
Physics

Presented in Partial Fulfillment of the Requirements
for the Degree of Master of Science at
Concordia University
Montreal, Quebec, Canada

August 2017

CONCORDIA UNIVERSITY
School of Graduate Studies

This is to certify that the thesis prepared

By: Avner Fitterman

Entitled: Learning-induced plasticity in vascular properties in the human brain

and submitted in partial fulfillment of the requirements for the degree of

Master of Science (Physics)

complies with the regulations of the University and meets the accepted standards with respect to originality and quality.

Signed by the final examining committee:

Laszlo Kalman Chair

Pablo Bianucci Examiner

Christophe Grova Examiner

Claudine Gauthier Supervisor

Approved by _____
Chair of Department or Graduate Program Director

_____
Dean of Faculty

Date _____

Abstract

Learning-induced plasticity in vascular properties in the human brain

Avner Fitterman

The brain is a plastic organ, able to undergo structural and functional changes following changing physiological contingencies, such as diseases and exercise training. However, the nature of the biological changes that underlie plasticity in the adult human brain is not fully understood.

In light of this lack of knowledge of the biological mechanism behind brain plasticity, non-invasive imaging can be used to track plasticity changes in the living human brain. Quantitative and physiologically-specific magnetic resonance imaging (MRI) techniques are an ideal tool to study these mechanisms. Plasticity is believed to involve a variety of physiological mechanisms. Some of these mechanisms are neuronal in nature, such as synaptogenesis and changes in neuronal morphology, but changes in non-neuronal tissue components are also thought to contribute, including angiogenesis. The latter may result in increased cerebral blood flow (CBF). CBF estimation can be obtained using arterial spin labeling (ASL). In this technique, water protons in blood are magnetically labelled and this labelling is used to measure the amount of blood that perfuses brain regions. The detection of blood perfusion changes during and following learning intervention would be indicative of a contribution of vascular plasticity to learning-induced changes. In this project, we will use ASL to measure plasticity-induced changes in CBF in motor areas during and following five days of motor task learning.

Author's contribution

The data acquisition took place at the Max Planck institution for human cognitive and brain science in Leipzig, so the author contribution was in processing the data and creating a pipeline for processing ASL data. The preprocessing was coded by the author on MATLAB, using FSL tools, as well as by developing his own algorithms, as was the case for the surround and sinc subtractions, the physiological filtering and creating the tSNR maps. For some of the subjects mapping for registration were created by the author, using algorithms developed by Pierre-Louis Bazin from the Max Planck Institute for Human Cognitive and Brain Sciences. Registration of CBF and tSNR maps to an anatomical space was done by the author using these mappings. Registration of these registered data to the MNI152 space was done using the flirt tool of FSL. Anatomical ROIs were created by the author. While the original functionally-defined M1 ROIs were created by another student at the Max Planck Institute, the author re-created ROIs for each subject at individual level analysis using FEAT tool of FSL. These ROIs were based on BOLD data and were registered to the anatomical space as well. The author also processed all the learning-related analyses.

Acknowledgements

I would like to show my gratitude to people who supported me during my MSc studies, especially:

- My thesis supervisor Dr. Claudine Gauthier for the opportunity to join her group, her valuable advices, her professional guidance, dedication and supportive attitude.
- Dr. Pablo Bianucci and Dr. Christophe Grova for accepting to be members in my academic committee and their kind support.
- My colleagues in Dr. Gauthier's lab group for their precious support, scientific discussions and for their friendly attitude.
- My colleagues in Dr. Grova's lab group for their kind support and the interesting discussions.
- Dr. Christopher Steele for the good advices.
- Dr. Laszlo Kalman for accepting to be the chair of my thesis defense and his kind support.
- Anna-Thekla Schmidt for the help with the data processing.
- Sophia Grahl for the help with information regarding the motor task.
- My parents who devotionally support me even though they live on another continent. This thesis is dedicated to them.

Outline

Chapter 1 - Introduction

1. Plasticity and Imaging – overview

In addition to the changes that occur in the brain as part of the development starting from the fetus, we now know that the brain is also capable of undergoing changes and reorganization in response to changing contingencies during the life span of a human [1]. Those contingencies may be of different types and time scales, and include recovering from diseases, learning and the adaptation to a shifting lifestyle. The development of brain imaging techniques has enabled the investigation of the impact of changing contingencies on the human brain. These imaging studies have provided accumulating evidence for the presence of plasticity-induced changes. Yet, the way this plasticity is implemented in the brain remains an open question. Animal studies allow us to characterize plasticity mechanisms with greater specificity, as more invasive tools are at the researchers' disposal. In the case of human studies, this issue becomes more challenging, as the main tool of research is non-invasive brain imaging.

Fundamentally, any imaging modality is sensitive to a specific physical mechanism, and each modality in isolation may provide only a limited amount of plasticity-related information. More specifically, in magnetic resonance imaging (MRI) the contrast is dependent on the different time decays of electromagnetic radiation sources due to differences in the environment, and cannot typically be used as a direct measure of a desired biological or physiological parameter. Nevertheless, MRI can be sensitive to certain components in the brain, such as blood, thanks to the magnetic properties of these components. This sensitivity to the blood compartment is the base for functional MRI (fMRI), as well as other techniques more specific to the cerebral vasculature. The goal of fMRI is to infer on the neural activity, which is the core of brain function, by acquiring time-series of images while this activity is expected. However, in MRI this kind of assessment can be obtained by the vascular response to the neural activity, rather than

directly. Hence the importance in the validation and improvement of fMRI technics by which vascular properties can be assessed.

MRI thus enables the extraction of both functional and structural information. Moreover, being non-invasive, MRI consists a promising avenue in both clinical and research usages. In particular, it is a convenient tool for better characterizing plasticity-induced changes. Quantitative MRI techniques can be exploited to more accurately study specific plasticity-related processes. Notably, a method for computing cerebral blood flow (CBF) will be used in the studies presented here. The main part of this thesis explores the CBF changes during learning of a motor task, which forms part of a larger multimodal ultrahigh field MRI study. Additionally, this thesis will present work on a quantitative fMRI technique as part of another project, in which an exercise intervention is used to induce brain changes.

2. Background

2.1 Animal Study

Physiological and biological changes during learning or physical exercise are the subject of extensive research, of which a significant portion is done on animals. Although animals have some limitations when used as a proxy for the anatomy and function of the human brain, animal studies have the eminent advantage of being easier to control. Controlling for effects of no interest poses significant challenges in human studies as the effect studied is typically mixed with confounding factors in any given intervention. For example, the challenge in examining the effect of exercise on the human brain is not only the difficulty to quantify the amount of exercise carried out by the subject, but also to exclude the effect of social interaction that may also affect the physiological parameter studied. Besides the possibility to better monitor and control animal behavior, more invasive methods can be implemented, allowing us to measure information on a cellular level. Histology staining techniques and electrical neural recordings are among the methods available in animal experiments [2-3]. In plasticity studies, histology might be

especially valuable as it is possible to count the numbers of neurons or synapses, for example. These biological parameters are not accessible by MRI, as the signal sources in standard MRI are averaged on the scale of millimeters. One drawback that exists however in invasive methods is the inability to continue with the intervention after performing the invasive procedure. Thus in many cases, a group of animals is required for each time point.

2.1.1 Evidence for the relation between physical activity and improved cognition

Animal studies have been instrumental in establishing that changes in behavioral function, such as skill acquisition, are manifested and supported by biological and physiological changes in the brain. More precisely, several studies investigated a possible relation between exercise and improved spatial cognition in rodents [4-6]. In these experiments, a group of rodents with access to a running wheel, is compared with a sedentary group. Fitness of the rodents is assessed by measures such as the number of wheel revolutions and heart weight. Following to this period of exercise, their spatial cognition is examined by inspecting their performances in a Morris water maze (MWM). The interpretation of the results from these studies has to be carefully considered, as many factors may be involved in determining group differences. For example, the advantage of the physical benefits that the exercise group over the control group should not be confounded with improved cognition when evaluating the rodents' performances in the MWM. After taking these factors into consideration, these experiments showed a positive correlation between exercise and performance in the MWM, indicating plasticity-related improvement in cognition.

Nevertheless, these experiments reveal little regarding the specific exercise-induced biological and physiological changes which enhance maze-related cognition. However, the involvement of certain biological processes that may support these changes can be tested. Some plasticity mechanisms thought to be involved are mediated by the Brain-Derived Neurotrophy Factor (BDNF) protein. This protein acts on hippocampal neurons, an area associated with the ability to form a "cognitive map" of the environment. By injecting a substance that mimics the BDNF receptor in the

hippocampus, the effect of this protein can be suppressed. Exercise-trained mice receiving this BDNF inhibitor were shown to performed in the maze equally poorly as a control group that did not exercise and did not receive the BDNF inhibitor [7]. This result suggests BDNF is involved in mediating exercise-dependent plasticity, though it does not imply that this process is sufficient. Changes at this molecular level are detectable only indirectly and are not accessible using conventional MRI.

Animal studies have however also shown changes at the macro scale. Other biological factors thought to contribute to learning-induced plasticity were suppressed to demonstrate their role. Kerr *et al*. tested two contributing mechanisms to enhanced learning ability in rats: neurogenesis (the formation of neuron cells) and angiogenesis (the formation of vessels) [8]. Kerr *et al* found that a group of rat receiving a neurogenesis inhibitor achieved the same improvements in a MWM following an exercise period as a group that did not received the inhibitor. On the other hand, a group that received an angiogenesis inhibitor performed as poorly as a sedentary group following an exercise period. This suggests that the enhanced ability to memorize a path in a maze is not supported by formation of new neurons, but may require the formation of new blood vessels. Although the findings of this study clearly support the role of cerebral vasculature as underlying mechanism of performance alterations, this study alone provides limited evidence for the contribution of exercise to changes in the vasculature. The limitation stems from the fact that the angiogenesis inhibitor damaged the rats' ability to run, causing them not to reach the required amount of exercise.

2.1.2 Association between exercise and cerebral vasculature

Other studies demonstrated relation between enhanced exercise and changes in cerebral vascular properties [9]. Swain *et al.* indirectly assessed changes in blood volume in the motor cortex following 30 days of physical training [10]. A group of exercised-trained rats presented higher deoxyhemoglobin (dHb) level and thus presumably higher blood volume in the region of interest. To further investigate vascular changes, cerebral blood flow (CBF) was measured during a hypercapnia challenge (while elevated levels of

CO_2 are inhaled by the animal). This procedure, which was also done following the exercise period, serves as a biomarker of cerebral vascular reactivity (CVR). The assumption is that brain vessels possess certain capability to dilate as a response to increased levels of CO_2. This ability is considered to be an indicator of the cerebral vascular function. Swain *et al.* found an increased CVR in the exercised-trained rat group. Although this finding might suggest improved vascular health, the author mentioned the possibility that changes in blood flow during hypercapnia are attributable to regular changes in blood CBF, rather than to the hypercapnic challenge. Although impaired CVR may be associated with poor cerebral health [11], some recent unexpected findings suggest that the relationship between CVR and vascular health may not be as simple as linear relation [12].

Given this evidence for exercise-induced vascular plasticity, it may be expected that similar effects on the vasculature obtained by pharmaceutical means can be also obtained by exercise. Zhang *et al* investigated potential contribution of exercise to vascular recovery following a stoke [9]. Using a stroke model in rats, the influence of an exercise period on vessels recovery was examined. In stroke, the cells on the edges of a cerebral ischemia created by a stroke, also referred to as the “ischemic penumbra”, retain their metabolic activity despite suffering from an impaired blood flow. This leads to cell death in this penumbral region. A thrombolytic reagent may increase the blood flow into those areas, thereby saving brain cells. However, this procedure is temporary and involve sides effects. In this study, physical activity was shown to increase blood flow in the region of the stroke, thereby improving functional recovery of cells without the aide of pharmaceutics.

2.1.3 Vasculature and motor learning

Exercise can be also regarded from the motor activity point of view. Although motor cortex activity was found during automated movements such as walking [13], it is often assumed that this kind of physical activity is associated with neural circuits comprising subcortical components and the spinal cord [14]. Thus the expected effect of

these automated movements on the brain will be in general more global. However, when the physical activity is not done automatically and requires skill acquisition, such as acrobatics, distinctive plasticity effects emerge. The root of the distinction is that learning that is involved in performing tasks of higher complexity, but not during exercise. Comparison between mere exercise and acrobatic physical activity of rats was done by Black [15]. The on-going improvement which was observed in the acrobatic learning group implied the existence of a motor learning process, which was in contrast to the static ability level of an exercise group using the running wheel. In terms of brain measurements, Black examined the paramedian lobule in the cerebellum, an area which is involved in fine adjustment of movements, as well as motor learning, among other functions. Purkinje cells, which are a type of neural cells, have a major role in the learning process [16]. It was found that learning was positively correlated to the number of synapses per Purkinje cell. Exercise, on the other hand, was characterized by angiogenesis in that area. The model offered by the authors to account for the different nature of those two effects relates to the nature of the physical activities and their energy demands. In the case of repetitive movements as in exercise, the intensive activation of the same neurons required enhanced energetic support without changing much the neural structure. In the motor learning group, the level of physical activity remained low. Instead, the acquisition of new motor skills required novel patterns of neural activity, thereby giving rise to new synapses.

2.1.4 The context of this study

Despite these associations proposed by Black of exercise with vascular plasticity and motor learning with neural plasticity, it will be argued that the plasticity induced by motor learning also has a vascular component. Although the effect of exercise is expected to be related to more global vascular changes, the main hypothesis of this work is that those changes are supported by a vascular component which is manifested through blood flow changes, regardless of the specific nature of the changes induced by motor learning in the motor cortex.

2.2 Human studies

2.2.1 Effects of exercise on cognition in aging brain

It is well established that the aging brain goes through anatomical and functional changes. Several studies have demonstrated that the anatomical changes are characterized by a loss of both grey and white matter volume. Functional changes, tracked using fMRI and positron emission tomography (PET), are characterized by reorganizations in activity pattern, among other changes [17-20]. Furthermore, these alterations may be related vasculature. The interdependencies of vasculature with the factors mentioned previously are not fully understood, and their interpretation is an on-going challenge. The association between cerebrovascular properties and aging were studied across several decades using PET, as well as MRI. Nevertheless, the relation between cerebrovascular health (in terms of CBF and CVR) and aging is still poorly known, with large variability results, despite several studies demonstrating decline in cerebrovascular parameters with age [21-23].

The aging brain is associated with cognitive decline. Because life expectancy of the global population has been significantly increasing over the passed several decades, there is an increasing interest to address the causes of the decline in cognitive performance with age, as well as finding approaches by which those effects can be mitigated. The notion of the brain as a plastic organ gives rise to the possibility of provoking alterations that improve cerebral health. This possibility raises the question: what lifestyle should be adopted to divert the course of the cerebral health from the expected decline during aging? One of these approaches relates physical activity and fitness to the prevention of cognitive decline [24]. However, despite the bulk of literature demonstrating a positive effect of exercise on cognition, much ambiguity still exists. The ambiguity, and findings which sometime suggest insignificant correlation may be attributed to the vast variety of parameters considered in different studies, as pointed out by Cox *et al* in his review [25]. More importantly, these studies may not in fact be examining the exact same phenomenon as there is considerable implementation and technical variability across

studies. In other words, the definition of “exercise” or “physical activity” may vary from one study to another. The way those definitions are realized depends, of course, on the training programs the subjects are going through, but also on the training program of the control group. The presence of an active control group allows a more refined interpretation of the results and can help us determine the best type of intervention for improving cognition.

This inconsistency in the existent literature and the still unclear relationship between exercise and cognition arising from the variability in control interventions make it necessary to use controlled interventions to identify the fundamental mechanisms that underlie the relationship between exercise and cognition. It has been suggested that the effects of physical activity on the brain occur at two levels [26]. At the molecular level, growth factors are released into the brain and facilitate processes of neuroplasticity [7]. This aspect of the effect of exercise was briefly addressed when BDNF was mentioned in the context of animal studies. The second level, one which will be more relevant to this work, is a supramolecular level, referring to neurogenesis and angiogenesis. However, neurogenesis in adults has so far only be demonstrated to occur in the hippocampus [27]. Angiogenesis, on the other hand, may comprise other vascular properties, such as blood volume and blood flow. The knowledge about angiogenesis arrives mainly from tumor researches, where dramatic increase in angiogenesis is observed [28]. The relationships between these and other vascular properties such as vessel density and capillary flow is complex however, often obligating researchers to impose important assumptions on their models. Moreover, angiogenesis, or any change in vascular properties may imply other, more fundamental neurobiological change, such as in the neural activity. This change in turn needs to be supported energetically by means of adaptations in blood supply to the relevant area.

Evidence for an association between fitness and cognition mediated by changes in vascular properties was reported by Brown *el al* [29]. In this study, two vascular properties were evaluated against age, fitness and cognitive level: cerebrovascular conductance (CVC) and mean arterial pressure (MAP). CVC gives an indication of the inverse of the

resistivity of arterial blood flow as it enters the brain. These parameters are measured using Doppler ultrasound to assess blow flow velocity. The expected relations of these parameters with age were observed, namely an increase in CVC and a decrease in MAP. More interestingly, age seemed to play similar role as the non-physical active lifestyle among the participants, as higher values of CVC were found in the physically active group compared to the sedentary, and lower MAP in the physically active group compared with the sedentary group. Being able to correlate cerebrovascular properties to cognitive level may provide evidence for the notion that vascular plasticity is the connecting link between fitness and cognition. This correlation, however, was found in this study to be non-significant. On the other hand, the same cerebrovascular parameters were found to correlate with cognitive level when measured via elevated values of CO2 (hypercapnia) in the blood. Brown speculated that at resting state (i.e., at baseline conditions), natural fluctuation in vascular properties conceal these relations.

Although these finding provide important information, by using imaging modalities such as MRI and PET much more specific information regarding vasculature, but also cerebral metabolism, can be obtained. For example, Local blood flow may be assessed over particular regions of interest (ROI). In the context of cognitive performance, these regions may be the frontal lobe, but also the hippocampus for its association with memory and spatial cognition [30]. The hippocampus has been the focus of several studies, including a study by Maass *et al* [31] showing a link between exercise and cognition. In his study, hippocampal blood perfusion was evaluated by an MRI technique that uses gadolinium as a contrast agent for perfusion. Hippocampal blood perfusion and performance on memory tasks were assessed before and after period of 3 months of aerobic exercise training. When comparing the two time points, increase in hippocampal perfusion and performance on the tasks were found in the younger participant but not in the older participants (the age range was between 60-77 years). That suggests that although the capability to plasticity-induced changes is degraded above certain age, it still exists in a relatively advanced age.

2.2.2 Activation patterns and functional MRI (fMRI)

While the findings from the resting state described above tell us about the overall relationship between physical activity and brain health, they do not provide information regarding the function of relevant brain regions, namely changes in activity patterns. Other issues may emerge when characterizing the neural activity of a cognitive task in aging. It has been shown that the intensity [32], as well as bilateral [19] neural activity increases with age, probably as part of a compensation mechanism for age-related processes occurring in the brain. This kind of reorganization of brain activity during aging will be readdressed in the context of motor learning.

The neural activity can be evaluated indirectly by the same parameter of blood flow used in the study by Maass, for example, but also in terms of blood oxygen level dependent (BOLD). These methods are related to the neural activity through the need to sustain this activity energetically. The mechanism by which the energy demand changes is met is based on blood flow increase in the relevant areas for supplying more oxygen, thereby diluting the deoxyhemobglobin (dHb) content in the blood. The BOLD signal, being sensitive to that dilution is thus increasing. Not only is the relation between energy demand and neural activity complex, but the oxygen level, besides being dependent on the oxygen consumption rate, depends also on the local blood flow and blood volume. Finally, another factor which is not taken into account in the BOLD measurement is the baseline oxygen level. Many factors my affect this baseline, among them are the parameters of which their effect is under question, and yet BOLD measurement is not sensitive to it.

2.2.3 Calibrated functional MRI

Given the difficulties in interpreting the BOLD signal in terms of neuronal activity, calibration methods were developed. In these methods, simultaneous BOLD and CBF measurements are used for evaluation of cerebral metabolic rate of oxygen ($CMRO_2$). These methods require additional measurements during a gas manipulation, to estimate a calibration parameter called M, representing the local BOLD signal that would have

been obtained in case of complete elimination of deoxyhemoglobin. This parameter provides the missing link between the seemingly arbitrary nature of the BOLD baseline and a value with a clear physiological meaning, CMRO2. The original method, developed by Davis *et al*, used hypercapnia, which is known as vasodilator, to estimate M. Vasodilation causes increase in blood flow, thereby increasing the BOLD signal [33]. The increase in these two parameters is needed for M assessment. An alternative approach uses hyperoxia, which causes an increase in the BOLD signal due to the elevated level of oxygen [34]. It is considered as a more direct approach, as the oxygen inhalation causes an increased level of dissolved oxygen in the blood, pushing the physiological conditions towards the state where deoxyhemoglobin is eliminated. Finally, Gauthier *et al* developed a generalized calibration method in which CMRO2 can be extracted regardless of the type of the gas used [35]. Acquiring two separate measurements using two different gases, further enables to assess CMRO2 in physical units, as well as oxygen extraction fraction at resting state [36].

In another study from 2012, Gauthier *et al* demonstrated the utility of hypercapnia-based calibration method by refining BOLD interpretation in the context of age-related changes [37]. Young and older adults participated in this study designed to investigate differences in neuronal responses between the two groups. The performance level in the Stroop task (a cognitive task designed to test the inhibition executive component) chosen for this study is known to be sensitive to the age-related cognitive decline. BOLD and CBF MRI measurements were acquired during the task and during hypercapnia for the implementation of the generalized calibrated method for assessing relative $CMRO_2$ ($rCMRO_2$) [35]. Despite differences in task performance between older and young adults, no significant differences were observed for the BOLD response or the CBF response during the Stroop task. Given a naïve interpretation of the BOLD signal, one could conclude that similar neuronal activity was present in both groups. However, since neither the scale nor the baseline are known, this conclusion would not necessarily be correct. The M value, obtained by acquiring additional measurements under a hypercapnic condition, provides this required scale. Lower M values were found for the

older group over various task-relevant ROIs, suggesting that different oxygen consumptions in the two groups gives rise to the same BOLD signal due to underlying physiological differences.

BOLD signal calibration methods by gas manipulations still suffer from several major disadvantages. The need for additional measurements acquired during gas manipulation make this procedure difficult to implement in several contexts. This is due partly to a possible discomfort for the participant. The main issue however, relates to the sensitivity of the method to measurements characterized by large error [38]. That in turn, leads to large variability in the resultant CMRO2 assessment. BOLD measurement is subjected to many uncontrollable factors, either physiologically-related, or instrument-related [39]. The CBF measurement originated essentially from the same type of scan as the BOLD, and thus suffers from the same drawbacks, except that those are magnified considerably by the fact that perfusion is weighted by subtracting two scans. By using one acquisition with gas manipulation, only a ratio of the CMRO2 during task can be assessed, relative to CMRO2 during baseline. This type of assessment involves 4 noisy measurements (BOLD and CBF during baseline and activation), causing the large variability in the relative CMRO2 measurement. For assessing absolute value CMRO2 with physical units, another set of measurements is included in the processing, further increasing the variability. It is for this reason that the CMRO2 values are averaged over a certain ROI rather than assessed voxel-wise. Each dimension in the 3-D ROI should be larger than the size of a voxel. Baseline measurements can be averaged over the entire cerebral cortex to provide enough signal averaging to obtain stable results, thereby however loosing the spatial specificity of the measurement. However, this kind of choice becomes more problematic for participants of higher age, as atrophy may reduce cortical depth to the level of voxel dimensions [40]. The tissue of interest in that case may only partly fill the voxel, typically causing an underestimation of the quantity measured. Furthermore, for modeling the BOLD signal, predefined parameters are used for describing the relation between bold response and magnetic susceptibility, as well as the relation between blood volume and blood flow. The optimal values for those parameters

are hard to determined as they vary as a function of the experimental setup, such as field strength [38,41].

In this study, a calibrated fMRI method is not discussed, however, it relies on CBF measurement which is in the center of this study. It therefore provides a motivation developing a CBF pipeline which can also serve in calibrated fMRI studies.

2.3 Motor learning

2.3.1 The multi-model plasticity imaging project

This project will focus on MRI data acquired at the Max Planck Institute for Cognitive and Brain Sciences in Leipzig as part of the multi-modal plasticity imaging (mMPI) project. The objective of the mMPI project is to characterize cerebral changes during and following learning of a motor task, while utilizing 7-Tesla MRI techniques that provide information beyond the information obtained using standard MRI. Five main modalities are exploited: quantitative susceptibility mapping (QSM) permits the construction of a vascular map [42], Diffusion Tensor Imaging (DTI), for obtaining tractography [43-44], quantitative T1 mapping, permits segmentation of cerebral cortices by utilizing their distinctive T1 values [45], and resting state fMRI, enables analysis of hemodynamics during resting state [46]. Finally, the method which will be in the center of this project, Arterial Spin Labeling (ASL), permits the assessment of CBF. The general hypothesis of the mMPI project is that the learning of a motor task across a few learning days will evoke changes in the brain, notably in the motor cortex [47].

2.3.2 Body part representation in the motor cortex

It is well established that the organization of the brain function has a local component, namely, an association between brain region and a certain function. In the case of the sensorimotor system, this feature emerges quite naturally from the structure of the axonal network from the peripheral nervous system to the white matter tracts that reach the cerebral cortex. As afferent axons ascend from receptors near the skin to the brain stem, they assemble together in the spinal cord in a way the preserves the spatial

information of the different body parts with respect to each other. This topographic representation is preserved all the way up to the somatosensory cortex. The different body parts are therefore mapped onto this part of the cerebral cortex, and due to tight a relation between the input of sensory information and the output of motor information back to the different body parts, this representation appears also in the motor cortex (MC), anterior to the somatosensory cortex [48]

Hence, each body part has a certain area of representation in the motor cortex, namely, an area that is activated when a subject is engaged in a motor task that requires a movement of that body part. Studies showed that there is an association between the ability to control a certain body part, and the size of its representation [49]. A different but related issue is whether this relation exist, not only with respect to different body parts within the same subject, but also for the same body part (which is involved in a certain motor skill) across different subjects. In other words, is there a relation between the MC representation extent and the skill level on a learned motor task? Studies have shown that certain areas in the grey matter and sub-cortices were found to a have larger volumes in expert populations, with a skill which is substantially more developed than in the average population [50]. In a study from 2003, Gaser *et al*. compared three groups different musical backgrounds [51]. A correlation between the level of musical skill (professional musicians, non-professional musicians and non-musicians) and grey matter volume was found across multiple brain regions, such as the superior parietal region, an area associated with integration of visual and sensory information.

2.3.3 The motor areas

As can be inferred from the study by Gaser et al., the sensorimotor system is not isolated from other brain areas. In fact, the motor cortex itself is composed of different subareas [48]. The different motor areas are connected with other cortices, implying the involvement of other brain functions, including higher order cognitive function [48]. The motor areas differ from each other also by the amount of output that they project. The primary MC (M1) is the main contributor to the cortico-spinal tract (CST), the main

pathway from the cortex to the spinal cord [52]. That is in agreement with the executive function of M1, namely, sending descending motor information to the different body parts. Other important areas in the MC are the premotor cortex and supplementary motor area (SMA) which also receives input from the prefrontal cortex and pre SMA, and contributes a little to the CST [53]. Activation which also involves premotor cortex and SMA activation on top of the M1, suggests the involvement of movement planning and, more generally, processing that involves cognition [53]. This kind of processing may be associated with an earlier stage of motor learning when the movement sequence is not yet performed skilfully.

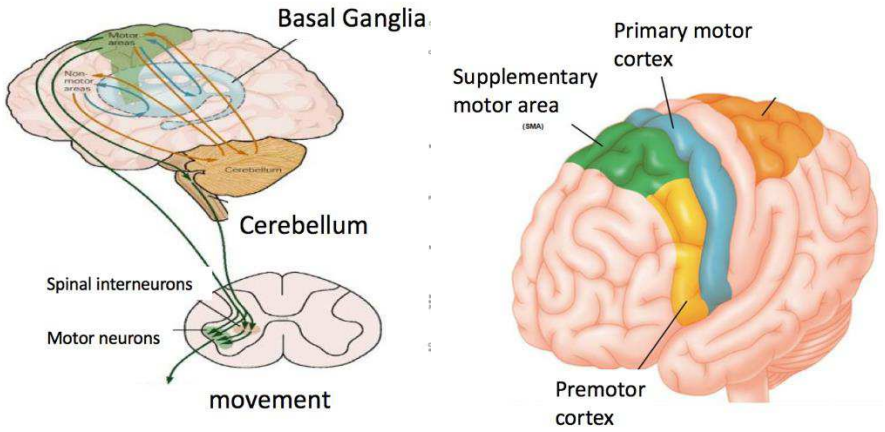

Figure 1.1. Left: Pathways between the three compartment involved in movement: Motor cortex, cerebellum and basal ganglia. Taken from www.slideshare.net/SubhadeepDuttaGupta1/sensory-motor-processing-in-planning-and-execution-of-movement. Right: Three of the subareas of motor cortex: primary motor cortex, supplementary motor area and the premotor cortex. Taken from www.dynamicbrain.ca/brain-anatomy-images.html

Thus the motor area contains several subareas, each one having its own neural architectonics and function. Motor learning animal and human studies have shown that neurons within the M1 population are capable of changing their function for encoding a newly acquired motor skill [54-56]. To investigate learning however, longitudinal designs

are more powerful than the cross sectional design used for example by the Gaser et al. study. The basic hypothesis may suggest that performance on a learned motor task (measured for example in terms of speed, correctness or synchronicity of movements) is positively correlated to the representation size within motor areas. This hypothesis was found to be partially true by Kleim *et al*. in the context of a rat study [57]. Two groups of rats were used, one that was learning a certain task and another that was physically active, but without any particular skill acquisition. Increase in the task-related representation area was found as expected, suggesting that more neurons in the M1 participated in the movement of body parts related to the acquired skill. However, the onset of this organizational change occurred at at later time point than the performance improvement with respect to improvements in performance. In addition, the synaptic density was found to be increased in the skilled group, but again, this change was not synchronized with the improvements in performance. Moreover, the improvement rate presented by the learning group was highest in the early phases of learning. By the third day their performance was significantly improved, while the change in representation and synapse density became elevated only at the 7th and the 10th days. The author however stressed that only persisting effects were examined, while the possibility of salient effect of the time scale of few tens of minutes was not ruled out.

3.4 Motor learning model

The last study shows that despite correlations between improved skill level and functional grey matter organization, any learning model should refer to other brain areas and mechanisms to fully explain how learning take place. In fact, there are two other brain compartments that have been shown to be involved in movement regulation. One of them is the basal ganglia (BS) which consist a collection of sub-cortical nuclei with pathways to cerebral cortices, including the motor cortex [58]. The other compartment is the cerebellum (CB), which also has connections to the cerebral cortex, notably the motor cortex, as well as input connections with ascending axons from the brain stem [59]. The CB has a role in motor functions such as movement adjustment, but there is also evidence

supporting its role in the learning process and particularly motor learning. This role arises from the special neuronal structure of the cerebellar cortex, which compares expected sensory information based on an output from the MC and actual sensory information. Learning emerges from discrepancies between these two sets of information. The BC and CB, together with the motor cortex are the main components of movement models [60].

In light of this knowledge regarding the role of the CB, BS and MC in movement production, researchers have been working to decompose the motor learning process based on different behavioral parameters and to associate learning components with the CB, BS and MC or combinations of them. In a typical motor task, there are two performance parameters measured: precision and reaction time. Similar to the two different time scales observed by Kleim, also in the time scale of days, the improvement in each one of those two learning performance components has been found to take place across different amount of time. Precision improvements have been found to precede the shortening of reaction time, which takes place at a slower rate. These finding reflect the idea of two learning stages [61]. An early stage, characterized by fast and explicit learning, when the movements require the involvement of cortices other than the MC as cognitive processes are involved, and a later stage, more gradual stage, in which the sequence of movement is optimized. Learning is often associated with another stage, in which the motor skill is improved without practice in a process known as consolidation [62]. In terms of brain imaging findings, the early explicit stage is characterized by a decrease in the cerebellar BOLD response, correlating with the decrease in errors, and providing support to the role of the cerebellum in error correction [62]. The optimization stage, on the other hand, is characterized by an increased BOLD response in M1 which may suggests functional reorganization of M1 neurons, as discussed in the context of the study by Gaser *et al* [51]. At this stage, less activation is detected in the association areas, pre MC and SMA, but more activation is detected in M1 [62]. This process of gradual restriction of the cortical areas of activity measured during a task to parts of the M1 area can be regarded as minimization of the resources. This is reversely analogical to the dispersion of the

activation area seen during aging, perhaps as part of a compensation mechanism to the reduced functionality of certain brain areas with aging.

3. The study's objective

In summary, there is a bulk of evidence concerning structural plasticity as well as the functional changes associated with it. The functional data acquired during motor learning research have so far mainly based on the BOLD contrast. As discussed in the context of calibrated fMRI and aging-related changes, there is however a need to better characterize vascular properties and thereby brain activity, since the BOLD response is related to CMRO2 (and therefore brain activity) through blood volume and blood flow. This interpretation ambiguity may also be problematic in the context of motor learning. Two main trends were pointed out, namely increase BOLD response in M1, and decrease in other motor cortex areas. Adding an evaluation of the CBF baseline changes in these areas will enable a better understanding the plasticity changes, but will also improve the neuronal interpretation of the BOLD response by providing additional information on the BOLD baseline.

To conclude, numerous studies have investigated the motor learning process and attempted to create a model describing the neural pathways and brain areas involved in this process and the way these compartments work together. However, the efforts to characterize these motor learning changes occurring did not fully exploit available MRI techniques to extraction relevant physiological information. For example, Gryga *et al.* have attempted to assess grey matter changes during motor learning. Using the same experimental paradigm as in this project, they demonstrated that changes in MC volume after learning were associated with performance [47]. However, there was no attempt to characterize grey matter changes in terms of physiological parameters. This is problematic, since changes in blood flow and vasculature have been shown to lead to artifactual volume changes [63]. As reviewed, CBF increases have reported following a physical activity, and according to a study by Chapman *et al*. [64], during cognitive

learning as well. Animal studies have not shown CBF changes during a motor task learning, but the limited scope of the available literature and the lack of CBF measurements in motor learning in humans require further investigation. The current work is thus based on knowledge acquired by studying various physiological processes which have not yet been merged into one experimental setup: on the one hand, the proven ability of the human brain for vascular plasticity following physical and cognitive interventions, and on the other hand, the induced grey matter changes demonstrated following a motor task learning, of which their neurophysiological interpretation remained unknown. This study both of those aspect by considering a vascular property in the context of a motor learning task.

Chapter 2 - Methodology

1. Theory

1.1 Principles of magnetic resonance imaging

1.1.1 Signal source

The source of signal in magnetic resonance imaging (MRI) is the magnetization formed by ensemble of magnetic dipoles in the presence of a high magnetic field. Each of these dipoles is the spin of a water proton. Although these dipoles are in the quantum scale, the fact that their number is of the order of magnitude of the Avogadro number, allows the formation of a detectable magnetization vector. However, the detection is not direct, and it becomes possible to detect the MRI signal by evoking time changes in the magnetization direction, and consequently causing the emission of electromagnetic waves. More technically, initially the sample is at constant high longitudinal magnetic field, which for paramagnetic materials, induces a net magnetization vector constant in time, pointing at the direction of the magnetic field. The application of a radiofrequency (RF) pulse evokes a rotation of the magnetization vector about one of the transverse axes. The angle of this rotation (the flip angle (FA)) is determined by the amplitude and duration of the RF pulse. As the magnetization acquires a transverse component, it rotates about the longitudinal direction, thereby emitting electromagnetic EM) wave at the precession frequency. The dynamics of the magnetization vector including its interaction with the EM wave is explained via the Bloch equations [65].

From the moment the magnetization is flipped towards the transverse plane, two simultaneous decay processes occur, which drive the system back to the equilibrium state. The more rapid decay among the two is associated with the dephasing of the spin rotations. The microscopic differences in the magnetic field across the sample cause the precession frequency of one spin to mismatch that of other spins. That, together with spin interactions, leads to increasing incoherence, and thus to a decay in the amplitude of the emitted EM waves with a time constant T_2^*. The order of magnitude of the decay time

constant is tens of milliseconds. The longer process of decay is of the longitudinal magnetization characterized by the time constant T_1, which is driven by spin-lattice interaction [66]. During this decay, the magnetization returns to its equilibrium orientation, namely, the longitudinal direction. To summarize, the transverse and the longitudinal components can be written as,

$$(1) \qquad m_{\perp}(x,y,z,t) = m_z^0(x,y,z)e^{-i\omega t-\frac{t}{T_2^*}}$$

$$(2) \qquad m_z(x,y,z,t) = m_z^0(x,y,z)\left(1-e^{-\frac{t}{T_1}}\right)$$

respectively, where $m_z^0(x,y,z)$, the local longitudinal magnetization at equilibrium, will be written from now on as $m(x,y,z)$, and ω is the Larmor frequency. Since the signal is proportional to the transverse component, the main interest will be in equation (1).

Two other time parameters, traditionally are time to recovery (TR) and time to echo (TE), indicate the time duration between the application of two successive RF pulses and the time between an RF pulse and the image acquisition, respectively. These parameters are thus determined by the experimentalist, depending on the desired contrast. Since T_1 and T_2^* depend on the spin environment, TR and TE can be set in such a way that will emphasize one aspect or another of that environment. For example, large molecule, such as those that exist in fat shorten significantly the TR. On the other hand cerebral spinal fluid (CSF) contain mainly water and thus correspond to long T_1. Setting a TR that capture this difference in the T_1 will lead to an image in which fat and CSF are highly contrasted. To eliminate the influence of different T_2^*, the TE is set to be as short as possible. Letting the TR to be as long as possible, allows the magnetization to fully reacquire its longitudinal magnetization, the dependence on the T_1 and T_2^* Is minimized, and the image is mainly affected by the density of the water proton. That is know as proton density weighting.

1.1.2 Image acquisition

The spatial encoding of the imaging in MRI is done by magnetic field gradients. The Larmor frequency is related to the magnetic field, and thus to the applied gradient $\vec{G}$, in the following way,

$$\omega = -\gamma(B_0 + \Delta B) = -\gamma\left(\omega_0 + \vec{G}\cdot\vec{r}t\right) \quad (3)$$

where γ is the gyromagnetic ratio of a proton, B_0 is the high longitudinal magnetic field (the magnet's main magnetic field) and $\vec{r} = (x, y, z)$. With gradients that change in time, eq. (3) becomes,

$$\omega = -\gamma(B_0 + \Delta B) = -\gamma\left(\omega_0 + \int_0^t \vec{G}(t')\cdot\vec{r}\,dt'\right). \quad (4)$$

When applying gradients, this phase has to be added to eq. (1), which will become

$$m_\perp(x, y, z, t) = m(x, y, z)e^{-i\omega_0 t - \frac{t}{T_2^*}}e^{-\gamma\int_0^t \vec{G}(t')\cdot\vec{r}\,dt'} \quad (5)$$

It can be seen from eq. (5) that the effect of the gradient is to modify the Larmor frequency. This fact is exploited to select a particular transverse slice in an image, by applying a gradient in the longitudinal direction. Only spins in the area along the longitudinal direction in which the magnetic field (which now varies along that direction) gives rise to a Larmor frequency within the RF pulse range, will be influenced by the pulse. Thus, the thickness of the slice is linearly related to the frequency range contained within the RF pulse. From now on, as the focus will be in a certain imaging slice selected as described above, the spatial encoding in the z direction will be disregarded.

The signal is composed of contributions from every point in the imaging slice. Therefore, the total signal is a spatial integration of eq. (5) (ignoring the decay term),

$$s(t) = \iint m(x, y)exp(-i\omega_0 t)exp\left(-\gamma\int_0^t \vec{G}(t')\cdot\vec{r}\,dt'\right)dxdy. \quad (6)$$

Since the scalar multiplication in the second exponential involves the coordinate vector, the expectation is that the term that is multiplied by this vector will be related to the reciprocal vector, traditionally denoted by $\vec{k}$. That suggests the following definitions

$$\text{(7)} \qquad \text{[illegible]}_x(t) = \frac{\gamma}{2\pi}\int_0^t G_x(t')dt'$$

$$k_y(t) = \frac{\gamma}{2\pi}\int_0^t G_y(t')dt'.$$

Moreover, the time variable of the signal can be always replaced by new variables, related to the old ones. The components of the reciprocal space vector that were defined in (7) can serve as such. This can be regarded as new representation of the signal. Instead of a one-dimensional representation, namely with the time parameter, each point in time will correspond to the two components in the new two-dimensional representation of the signal. This two-dimensional space is referred to as k-space, which here is denoted with $S(k_x, k_y)$.

The signal equation can be viewed as a two dimensional Fourier transform of the longitudinal magnetization, and in the k-space coordinates can be written as,

$$S(k_x, k_y) = \iint m(x,y) exp(-i\omega_0 t) exp\left(-i\left(k_x x + k_y y\right)\right) dxdy. \quad (8)$$

The information regarding the sample is buried in $m(x, y)$, since it is proportional to the proton density. Essentially, an MRI image is a proton density weighted map that can be further weighted using different time parameters such as T_1 and T_2^*. Hence the image itself can be obtained by an inverse Fourier transform of the signal in k-space

It is evident From equation (8) that an MRI acquisition comes down to filling the k-space (i.e. signal sampling using variable values of $\vec{k}$ corresponding to different combination of x and y gradients). Consequently, there is a perpetual effort in MRI to sample as many points in k-space as possible during the acquisition. There are, of course, infinite ways of filling the k-space [67]. One may choose, for example, to use a large values of $\vec{k}$, while having a large sampling time, namely, large intervals between two adjacent $\vec{k}$ values. That will correspond to a high resolution image with a small field of view (FOV). Moreover, the trajectories in k-space may be varied according to the needs of the specific image acquisition. Using $\vec{k}$ values from the edges of the k-space at higher sampling rate will emphasize the fine details of the image, but will reduce its intensity. Signal obtained using small $\vec{k}$ values gives rise to larger intensity with smaller sensitivity to fine details. These signal manipulations are part of the notion of a pulse sequence design, a domain in which parameters, such as those related to timing, associated with RF pulse applications are determined according to specific interests.

The signal is related to an electromotive force induced on an electric circuit in a relation given by Faraday's law. According to Faraday's law, the electromotive force is minus the time derivative of the magnetic flux through the circuit. In MRI, the circuit is part of a receiving coil, and the magnetic flux is the surface integrated local magnetization, as it is considered to be the only time varied contribution to the magnetic field. The voltage induced on the coil consists the MRI signal is the measured quantity. Later it is amplified and digitalized such that it could be analyzed.

1.1.3 7T-Tesla MRI

The motivation for using higher magnetic field emerges from the relation between the magnetization and the external magnetic field. Under the assumption of linearity, the total magnetization M is related to the external magnetic field H according to,

$$\vec{M} = \chi_m \vec{H}, \quad (9)$$

where χ_m is the magnetic susceptibility of the sample. For MRI purposes, given the nature of body tissues, the magnetic susceptibility may be treated as a scalar despite the fact that as the magnetization vector may not point at the same direction as the external field, it may be a tensor quantity. Since the susceptibility relates sample properties and magnetization (and hence the signal), it often has an important role as a biomarker of physiological information, such as vascular information [68]. A higher field will enhance signal differences created by susceptibility differences, thereby emphasizing this kind of information. On the other hand, susceptibility differences may emerge also from factors of no interest, causing degradation of the image quality. For example, at the interface between between two different materials. An example from the context for brain MRI, is the interface between the air in the nasal tunnels and bones, creating a signal loss around air-filled sinuses which worsen at higher field strength. Other challenges associated with susceptibility as well as the utilization of susceptibility differences will be addressed further, mainly in the context of functional MRI (fMRI).

Another challenge associated with the use of higher magnetic fields is inhomogeneity in the received field. As the EM wave travels from the sample to the coil,

its amplitude changes at the rate of the proton Larmor frequency, whereas spatially it does not change much. The proton Larmor frequency at 7T is around 100 MHz which gives rise to a wavelength of about few meters in a vacuum. Although shorter than the wavelength of lower field scanners, that wavelength justifies the assumption of a spatially constant magnetization. However, when a sample is considered rather than vacuum, the electromagnetic wave velocity decreases, and thus the wavelength might be reduced to a few tens of centimetres, namely, the order of magnitude of the brain. In that case the assumption of constant magnetization field across the sample is not completely satisfied, causing possible distortions in the image. A similar argumentation can be applied for the B_1 field, the amplitude of the exciting RF pulse applied by the transmitting coil. For correcting the effect of the spatially varied magnetic field, multiple coil elements (channels) are often used to acquire the signal or to transmit simultaneously. The combination of different channels allows a better coverage of the B_1 field, thereby increasing the B_1 field homogeneity.

1.2 Arterial spin labeling (ASL)

1.2.1 Blood flow measurement – review

Blood flow is a measure of the blood volume (including the plasma) that enters a certain region per unit time. The region may be a voxel and the flow may contain intra- and extra-vascular components. When the extra-vascular component is taken into account, there is an interest in the amount of flow per certain amount of tissue. Thus the units in that case will be flow per unit of mass, and although the terms flow and perfusion will be used interchangeably, in the context of MRI, only the definition of flow per unit mass will be used [69], unless stated otherwise.

Certain imaging modalities have the capacity to assess blood flow. In ultrasound, the Doppler effect is at the core of the technique. Standard Doppler ultrasound exploits reflected sound waves from surfaces between two apparatus and time differences between emitted and received waves in the transducer. For flow measurement, the different wave length received from moving targets permits an assessment of its velocity.

The method, however is effective for high velocities such as in large vessels, and not sensitive enough for blood velocities in capillaries, for example.

In other imaging modalities, such as positron emission tomography (PET) and single photon emission computed tomography (SPECT), a radioactive bolus of labeled water is injected into the blood. By scanning the subject in a detector sensitive to the radiation emitted by the bolus, highly sensitive map of the bolus concentration can be obtained. By considering the time profile of each voxel, blood volume and blood flow maps can be constructed. Similar concepts underlay endogenous MRI CBF measurement techniques. However, the physical principles underling the signal production is different. Instead of emitting radiation, the bolus is an MRI agent contrast, typically gadolinium. Since gadolinium is highly paramagnetic, it increases R_2^* significantly, thereby creating a loss of signal in the vessel where it passes. The loss of signal can be treated similarly to the signal originating from the radioactive bolus in the case of PET and SPECT. ASL, on the other hand, is a noninvasive method — no contrast agent is required for creating the flow contrast. An advantage of ASL is that it can be used to measure tissue perfusion rather than vessel flow. This is because the bolus in contrast-agent techniques cannot penetrate the blood-brain barrier, and thus these techniques do not contain the extra-vascular component in their measurement.

The multiplicity of imaging method to quantify blood flow in term of physical units allows the validation of one method with respect to another. ASL by its self is a group of methods with significant variation in measured CBF. However, also across imaging modalities, the observed CBF values are in accordance with PET technique for blood flow measurement [70].

1.2.2 Basics of ASL

All ASL techniques are based on the acquisition of two images, one acquired a few seconds after the other. The two images are acquired identically, except for flow encoding in alternate images. The flow encoding is achieved by applying a 180 degrees RF inversion pulse prior to the acquisition of every other images (referred to as the tag images),

manipulating the longitudinal magnetization in certain areas and subtracting the two images. The position and orientation of the FOV should be such that brain perfusion is well captured. Such geometrical consideration will be further elaborated when the blood flow model will be discussed. Another pulse sequence consideration is the need to acquire the images quickly. Long acquisitions will fail to capture the blood flow, as will be discussed below. For this reason, echo planner imaging (consisting in filling of the entire k-space in one TE) is typically applied. Finally, the pulse sequence should be insensitive to any relaxation process, besides the one associated with the blood tagging. More specifically, axial magnetization decays are undesired, and thus mitigated by utilizing proton density contrast.

The area affected by the inversion pulse varies between different ASL methods, and for simplicity, it will be assumed that is applied below the ROI. After the application an 180^0 RF (inversion) pulse on the tagging area, the sources (typically blood's plasma) in that area flow into the ROI, while their magnetization decays back to the equilibrium state. A few seconds after the application of the inversion pulse, the tag image is acquired at a moment where the incoming flow from the tag area has reduced the net longitudinal magnetization in the ROI. The reduction in the net longitudinal magnetization leads to a reduction in signal in the tag image with respect to a control image, in which no saturation pulse was applied. The difference in intensity between the two originates from inflowing sources to the region of interest, and thus the subtraction image is a perfusion weighted image.

One of the main challenges in ASL is determining the duration between the inversion pulse and the tag image acquisition (post labeling delay, PLD) which optimizes the perfusion image in terms of artifacts and SNR. The actual value of this duration may vary as a function of various factor such as the strength of the magnetic field, anatomical properties and the ASL technique. However, some basic principles are valid regardless of these factors. This duration should leave enough time for the blood to flow from the tagging area to the region of interest. On the other hand, the image acquisition should be close enough to the moment of the application of the tagging pulse due to 2 processes:

the washout of the labeled blood from the ROI and the return of the longitudinal magnetization back to equilibrium state. In fact, the ASL pulse sequence is realizable because of the fact that the magnetization decay and the PLD happen to be of the same timescale. Because of this, using a higher field is beneficial in terms of ASL SNR, since a higher field prolongs T_1 values.

During the initial development of the ASL pulse sequences in the nineties, technological limitation associated with the rate at which gradients can be applied, often limites the acquisition to a single slice. However, utilization of EPI pulse sequence now enables multi-slice acquisitions of the entire 3-D ROI in one TR. The EPI acquisition scheme gives rise to the possibility to create perfusion data time series. The fundamental time resolution of that time series is twice the TR because of subtraction. EPI allows us to use a TR of a few seconds, keeping the time resolution high enough for functional MRI since the hemodynamic response is about 30 s and peaks around 6 s.

ASL can be used to measure the localized hemodynamic response that accompanies brain activity. Furthermore, perfusion imaging has an advantage over BOLD in fMRI for determining the exact localization of the activity. Since the BOLD response is highly dependent on deoxyhemoglobin (dHb) concentration, it is biased towards veins. These can be several centimetres from the actual locus of activity (71). Under the assumption that the energetic requirement for neural activity is related to blood supply into the area of activity, which is reasonable considering that the brain cannot store oxygen and glucose locally, and ignoring MRI resolution limitation, CBF maps should provide a good localization up to the length scale of the distance between capillaries and neuron cells.

Besides the difficulty to determine the PLD, perfusion measurements may include arterial blood that flows out of the FOV, instead of flowing into the capillaries. This bias is mitigated by a longer post-label delay before acquiring the tagged image. However, a longer PLD may cause a separate issue of decreased image contrast, related to T_1 decay. Therefore, the timing of the sequence has to be carefully chosen to minimize both sources

of decreased data quality. Models that seek to quantify the perfusion signal address these types of issues and will be discussed later.

1.2.3 ASL methods

ASL are typically categorized by the tagging method used. Three different types of RF radiation can be applied: continuous RF radiation (cASL), pseudo continuous radiation (pCASL) and an RF pulse (pASL). The latter will be in the focus of this project, while the other two will be briefly introduced.

The continuous RF radiation is applied below the ROI and selectively affects only moving spins, and is thus referred to as flow-driven inversion [72]. The radiation is applied to a narrow slab where a gradient field is also applied. The slab is placed at the level of the carotid arteries since all the blood to the brain transits through these arteries.The movement along the gradient creates the effective field which is correspond to the Larmor frequency, thereby permitting the radiation to rotate the moving spins by 180 degrees. The duration of the RF pulse should be long enough to permit the formation of enough tagged blood to cover the ROI once the tag reaches the brain. This parameter is thus strongly dependent on the blood velocity, but is usually set to 1-2 s. the amount of blood passing through the thin slab of the RF radiation correspond to the available perfusion signal that can be potentially produced. However, the tagging efficiency of this method is relatively low, and is typically about 80%. Another important disadvantage of this technique is that it causes high levels of specific absorption rate (SAR), which is a measure of the rate of the RF energy deposited in the tissues. Due to the limited amount of energy that can be safely deposited in tissue, this technique often cannot be used effectively.

Pseudo-continuous ASL has similar properties as CASL in terms of the tagging strategy, but is different with respect to the way the inversion is achieved. Instead of a continuous radiation, a train of 180 RF pulses is applied, namely, fast sequence of many RF pulses applied one after the other. The duration between two sequential pulses is of the order of milliseconds and the total inversion duration is similar to CASL. The lack of

continuous radiation significantly reduces the SAR level. Moreover, the tagging efficiency obtained by this method is higher, as the tagging achieved by 180 inversion pulses, rather than flow-driven inversion. It is for this reason that pCASL becomes the preferred method for acquiring perfusion images and is usually used in cases where it is technologically feasible.

A third method is pulsed ASL, which is a category of its own, as it may be implemented using different tagging strategies. Ideally, the only effect that the inversion has on the spins is their rotation by 180 degrees. Realistically, however, the pulse is accompanied by other effects, thereby necessitating certain adaptations, which are realized by the different tagging strategies. A general goal in ASL is to maintain the same conditions in the tag image acquisition as in the control acquisition, excluding the tagging effect. This kind of control is difficult to achieve due to off-resonance effects in the ROI, created by the inversion pulse. Ideally for example, the inversion pulse does not match the Larmor frequency of spin in the ROI. However, the various chemical environment of these spins shift the Larmor frequency, thereby creating a distribution which may overlap the inversion RF pulse profile and causing spins to depart from the equilibrium state necessary during the acquisition. Among the spins which are in a dynamic chemical equilibrium with other components of the chemical environment, some will interact with the magnetization available at the Larmor frequency during the image acquisition. This process is known as magnetization transfer (MT) and the different tagging strategies aim to avoid this effect.

In the echo-planar imaging-based signal targeting by alternating radiofrequency pulses (EPISTAR) pulse sequence, the same inversion pulse applied below the ROI at the level of the carotid arteries for tagging inflowing blood, is also applied before the control acquisition above the ROI in a symmetric manner with respect to the ROI. The application of these two pulses cancels off-resonance effects. Another method is proximal inversion with control of off-resonance effects (PICORE) where the off-resonance inversion pulse (namely, a pulse without localizing gradient) is applied on all the brain before the acquisition of the control image. Once again, this method is designed to cancel off-

resonance effect. Lastly, the method that is used in this project is flow-sensitive alternating inversion recovery (FAIR). In this pulse sequence an inversion pulse is applied on the ROI in both the tag and control images, thereby preventing the MT bias. However, the inversion pulse is extended to cover the coil sensitivity area in the tag image (i.e. the full body for a body coil or the whole head for a head-only coil as used here), while the inversion pulse is localized to the ROI during the control image acquisition. In terms of the physical mechanism producing the perfusion signal, prior to the control acquisition, untagged blood flows into the ROI during the PLD and slightly increases the available magnetization relative to the tagged blood. The tag acquisition should produce similar signal in the ROI, expect for the small signal increase produced by the incoming flow during the control acquisition. Therefore, by subtracting the tag image from the control, a perfusion weighted image is obtained.

As a direct consequence of the way the tagging is achieved, the three methods mentioned above differ also in terms of the interpretation of the perfusion signal. The contribution to the CBF signal of blood flow entering the FOV from above may not be the same as that from below. In the case of EPISTAR, the inversion pulse prior to the control acquisition above the FOV, leads to a negative contribution from incoming blood from above the FOV. In the case of FAIR, as the pulse sequences of both the control and tag images are spatially symmetrical, blood that enters from above the FOV has the same (positive) contribution as blood that enters from below. In the case of PICORE, blood enters from above should not have any contribution to the perfusion signal [73].

1.2.4 Quantification

We know from the basics of MRI that the measured quantity is an amplified current produced by the effect of RF radiation emitted by the spins of water protons on a receiving coil. A priori, structural or functional information is always given by the relative intensity of a voxel with respect to other voxels. Certain contrast mechanism can highlight certain aspects, but the value of each voxel will not have physical meaning of itself. To convert the voxels' intensity to values that contain absolute physical meaning, a model

has to be formulated. That model can be regarded as a converter, namely, a function that receives the voxels' intensity and a reference intensity as its inputs, and returns values related to the original values, yet different and associated with physical units. The ASL quantification process was established by Buxton *et al*. [74], and is often referred to as the standard model for quantifying ASL signal.

As a first step, the goal is to find an expression for magnetization that consists of the ASL signal, and enters the voxel at time t, Δm_0, given the decay constant of arterial blood, T_1^b (the index is to clarify that it is at t=0 from the moment of entrance to the voxel). It is simply the difference between control and tag images. The magnetization of blood that starts entering a voxel in the control image, is also the equilibrium magnetization of arterial blood m_b. In the case of the tag image, the entering blood is affected by the inversion pulse, and thus the available magnetization is $m_b\left(1-2\alpha e^{-\frac{t}{T_1^b}}\right)$. Hence, Δm_0 can be described as,

$$\Delta m_0 = 2m_b\alpha e^{-\frac{t}{T_1^b}}, \quad (10)$$

where the ratio of the magnetization available for the ASL signal and the total magnetization is often denoted as,

$$c(t) = e^{-\frac{t}{T_1^b}}. \quad (11)$$

Once inside the voxel, there are two signal decay processes that are considered in the standard kinetic model: magnetization clearance and magnetization decay.

Magnetization clearance refers to the process by which magnetization leaves the voxel due the movement of the water proton spins. The arteriole walls are relatively thick, such that water does not flow out of the arteriole. ASL, therefore, is thought to detect perfusion in the capillary bed. In the latter, water is assumed to exchange freely between capillaries and tissue. Moreover, the diffusion of water into tissue is assumed to occur immediately as the blood reaches the voxel [75]. The rate of the arrival magnetization, namely the flow f is equal the the clearance rate by the diffusion (here, the flow is of volume of blood per volume tissue, and thus has units of frequency). A correction for the

fact that not all the voxel contains tissue, is accounted for by the inclusion of the ratio coefficient of tissue and and blood. Statistical dynamics dictates an exponential clearance, and thus the expression for the clearance term is,

$$(12) \quad r(t-t') = e^{-\frac{(t-t')f}{\lambda}},$$

where λ is the brain-blood partition coefficient. This represents the ratio of water that entered the voxel at time t', and is still in the voxel at time t.

It was implicit above that the water diffuses freely not only between blood and tissue, but also inside tissue. In other words, whatever the tissue might be, the assumption is that it is composed of a single compartment. This assumption also facilitates considerations of magnetization decay. It is assumed that once inside the voxel, the T_1 constant changes from that of the blood to that of tissue, T_1. In fact, the assumption of constant T_1 across the capillary bed is realistic also in the case where different compartments are involved, given that the water exchange between them is fast enough (as is assumed regarding blood and tissue). The ratio of magnetization left at time t with respect to the magnetization in the voxel at time t' is,

$$(13) \quad m(t-t') = e^{-\frac{t-t'}{T_1}}.$$

From these 3 functions, an expression of the ASL signal as a function of time can be constructed. Setting t=0 to be the time of the inversion pulse, at any time before Δt, the travel time of blood from the most proximate point of the labeling region to the voxel, the ASL signal in the voxel is zero. The moment tagged blood starts to enter the voxel, the dynamics is described by the convolution of the delivery function, *c(t)* and the multiplication of the functions associated with signal reduction, namely *r(t-t')·m(t-t')*. (The reason for the multiplication in the latter term is that each one of the functions, *r(t-t')* and *m(t-t')*, represents the portion of tagging left in the voxel while ignoring the other function). This is valid as long as tagged blood keeps flowing into the voxel. This duration is denoted by τ, and is estimated from the width of the tagging slab, given a certain blood velocity in that tagging area. Thus, assuming a constant flow over time, by multiplying this convolution by the flow, the ASL signal, is obtained,

$$(14) \quad \Delta m = 2m_b \alpha f \cdot \{c(t) * [r(t-t') \cdot m(t-t')]\},$$

or explicitly,

$$\Delta m = 2m_b \alpha f \int_{\Delta t}^{t} exp\left(-\frac{t\prime}{T_1^b} - \frac{(t-t\prime)f}{\lambda} - \frac{t-t\prime}{T_1}\right) dt' \quad (15)$$

This is valid for $\Delta t < t < \Delta t + \tau$. Equations (15) is a kinematic equation for the signal, in which the integration term represents the portion of tagging entering the voxel at time t, weighted by the tagging decay, and *f* corresponds to the rate in which tagging enters the voxel.

At later times, the delivery function should not by included in the calculation, and the expression becomes,

$$\Delta m = 2m_b \alpha f \int_{\Delta t}^{t} exp\left(-\frac{(t-t\prime)f}{\lambda} - \frac{t-t\prime}{T_1}\right) dt'. \quad (16)$$

After integration, the expression for the three time intervals are,

$$\Delta m = \begin{matrix} 0 & t < \Delta t \\ 2m_b f(t-\Delta t)\alpha e^{-\frac{t}{T_b}} q_p(t) & \Delta t < t < \Delta t + \tau \\ 2m_b f \tau \alpha e^{-\frac{t}{T_b}} q_p(t) & \Delta t + \tau < t \end{matrix} \quad (17)$$

where,

$$q_p(t) = \begin{matrix} \frac{e^{kt}\left(e^{-k\Delta t} - e^{-kt}\right)}{k(t-\Delta t)} & \Delta t < t < \Delta t + \tau \\ \frac{e^{kt}\left(e^{-k\Delta t} - e^{-k(t-\Delta t)}\right)}{k\tau} & \Delta t + \tau < t \end{matrix} \quad (18)$$

where,

$$k = \frac{1}{T_b} - \frac{1}{T_1} - \frac{f}{\lambda}. \quad (19)$$

Expression (17) can be simplified by considering the values of the different parameters. At high field (3T and above), the T_1 value of grey matter tissue approaches T_b [76]. The flow is of the order of 0.01 s^{-1} where □ approaches unity. These considerations guarantee that the factor $q_p(t)$ will be only slightly dependent on time, and thus can be set to 1.

So far, among the time parameters that were introduced, only one can be manipulated the pulse sequence: τ. Using a long bolus duration is beneficial, as it may result in equilibrium between incoming and outgoing tagged blood. During this time the ASL signal will be stable and equal to the maximal ASL signal that can be obtained in a given acquisition. This is the source of advantage of PCASL over other ASL techniques.

Unlike CASL, PCASL is not limited in the inversion pulse duration. PASL, on the other hand uses a short RF pulse, and the bolus duration is determined by the extent of the tagging slab. Therefore, in this case, the bolus duration is limited by the geometry of the RF coil.

T_1 values increase with magnetic field strength. The difficulties involved in using a higher field scanner were pointed out in the context of the basics of MRI, yet given this theoretical framework alone, higher values of T_1 are beneficial in ASL, as it results in higher ASL signal from reduced decay during the PLD. The slower the tagged spins inverted revert back to the equilibrium state, the larger the magnetization in the tag will deviate from that of the stationary spins. These consideration, regarding the bolus duration and T_1 are summarized in figure 2.1.

From equation (17), it is still unclear how to account for the transit time Δt. This parameter is difficult to evaluate, and is also spatially dependent. To address this issue, a few strategies were developed. One of these strategies consists in multiple subtractions between the tag and control images. Thus, instead of acquiring the pairs of tag and control images with the same time interval between the inversion of the image acquisition (time from inversion, TI), a time series of ASL signal is acquired, by alternating the TI values. In fact, equation (17) can be regarded as a set of equations, one for each time point. Since there are only two unknowns, f and Δt, two time points are sufficient. Nevertheless, producing a time series ASL signal with additional TI values can be used to validate for the model, in cases where the ASL signal, which is independent of the model, follows the theoretical curve given by eq. (17) [77]. Another strategy utilizes an additional pulse during the tag and control acquisitions, a saturation pulse that "resets" the blood labeling. In this method, quantitative imaging of perfusion using a signal subtraction (QUIPSS) [78], both the bolus arrival time and the bolus duration are eliminated from the calculation.

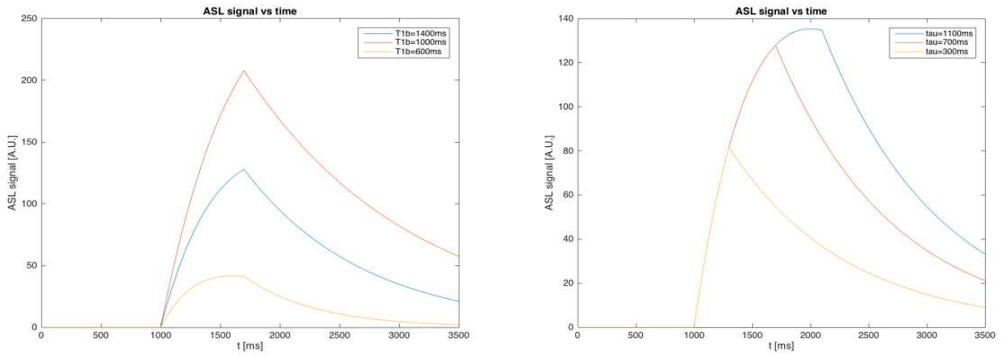

Figure 2.1. The theoretical curve of the ASL signal as a function of time, using variable time parameters.

1.2.5 Quantitative imaging of perfusion using a single subtraction (QUIPSS)

Although CBF quantification can be achieved using the described model and certain assessment of the time parameters, the QUIPSS pulse sequences may improve the accuracy of the procedure. Two different approaches may by used to implement the QUIPSS strategy. One of them uses a saturation pulse below the imaging slab, and in the other the saturation pulse is applied on the imaging slab.

By applying a saturation pulse on the imaging slab, before both the control and the tag acquisitions, the labeling of all the spins present in the imaging slab during the saturation pulse is eliminated. However, blood which enters the imaging slab after the saturation pulse will renew the labeling supply to the imaging slab. This period of renewal is known, since it is the moment of the application of the saturation pulse. It can be regarded as the moment when tagged blood starts flowing into the imaging slab. An a priori estimation of the bolus arrival time is required, but any estimate of this value will be sufficient, as long as it does not exceed the bolus duration. It is then provided that labeled blood will enter the imaging slab right after the saturation pulse.

The time duration between the saturation and the inversion pulse is denoted by TI_1, whereas to the image acquisition is denoted by TI_2. Thus, the conditions for the first QUIPSS method on these time parameters are,

$$TI_1 > \Delta t \qquad (20)$$
$$TI_2 < \Delta t + \tau$$

where the ASL signal for that case can be estimated as,

$$\Delta m(TI_2) = 2m_b(TI_2 - TI_1)f\alpha e^{-\frac{TI_2}{T_b}} q_p(TI_2). \quad (21)$$

The assumption of the first QUIPSS technique (QUIPSS I), that tagged blood is still flowing into the imaging slab, should hold also in the second QUIPSS technique (QUIPSS II), with the additional requirement that not all the tagged blood left the tagging area. Given that the saturation pulse is applied in this case on the tagging area, this is equivalent to the requirement that,

$$TI_1 < \tau. \quad (22)$$

With the saturation pulse applied to the tagging area, it is assumed that immediately after TI_1, no more tagged blood leaves the tagging area. TI_2 should be set such that during the acquisition, no more tagged blood enters the imaging slab. Given the fact that after the application of the saturation pulse TI_1 represents the bolus time, this condition is equivalent to the requirement that,

$$TI_2 > TI_1 + \Delta t \quad (23)$$

Under this condition, the ASL signal is given by,

$$\Delta m(TI_2) = 2m_b TI_1 f\alpha e^{-\frac{TI_2}{T_b}} q_p(TI_2). \quad (24)$$

The QUIPSS methods can be summarized by considering the two parts of equation (17) corresponding to the two non-zero parts. QUIPSS I consists of resetting the ASL signal at a time point that is within the first time interval, thereby eliminating Δt. Knowing the time of the image acquisition enables the usage of the equation that is valid in this time interval, an equation that does not contain the bolus duration. QUIPSS II consists of resetting the ASL signal at a time point within the second time interval, thereby eliminating τ. In this case Δt is absent from the equation. Thus, in both methods, both Δt and τ were eliminated from the calculations.

1.3 ASL data analysis

1.3.1 Subtractions

The flow-dependent signal from the ASL data must be isolated prior to quantifying CBF. The ASL signal will then serve as the input to the standard kinetic model in which CBF

is calculated (see theory section). A model for the assessment of ASL signal given a series of *N* interleaving tag and control images was formulated by Liu *et al* [79]. The following notation was adapted from Liu's study. Given a time series *y*[n] of interleaving tag and control images, the ASL signal at a time point *n* (where *n* = 1,2,3 … *N*) can be assessed by,

$$(25) \quad q[n] = [(-1)^{n+1} y[n+1]] * g[n],$$

namely, the convolution of the filter *g*[n] with the ASL signal with interleaving signs.

The choice of a filter determines the type of averaging performed over its window, as well as the weight given to each time point. A simple pair-wise subtraction (the subtraction scheme which was implicitly referred to when the ASL pulse sequence was described) will correspond to the filter,

$$(26) \quad g_1[i] = [1,1],$$

where the convolution is performed as,

$$(27) \quad q[n'] = \sum_{i=1}^{2} \left[(-1)^{i+1} y[n'+i]\right] g[i],$$

where n' is odd, or explicitly,

$$(28) \quad q[n'] = \begin{pmatrix} y[2]-y[1] \\ y[4]-y[3] \\ y[6]-y[5] \\ \vdots \end{pmatrix}.$$

Simple subtraction can also involve each time point from the raw data twice (except the 2 end points) to thus obtain an ASL signal composed of nearly the same number of time points as in the raw data. This can be described as up-sampling of the perfusion time course by interpolating the additional points. This type of filtering may be beneficial when time resolution is particularly important, such as the case when there is an activation expected during a certain time interval.

Pairs of tag and control can be also averaged if they are associated with the same perfusion time point. More specifically, a control time point can be subtracted from the tag time points of both sides. This kind of subtraction is known as a surround subtraction, and its filter is,

$$(29) \quad g_2[i] = [1,2,1]$$

where the explicit result of the convolution is,

$$(30) \quad q[n] = \begin{pmatrix} -y[3]+2y[2]-y[1] \\ y[4]-2y[3]+y[2] \\ -y[5]+2]y[4]-y[3] \\ \vdots \end{pmatrix}$$

lastly, a third type of filter is the sinc filter, defined as,

$$(31) \quad g_2[i] = sin(\pi i/2)/\pi i$$

in this case, any window width of the filter can be used, however, the time point will be weighted with a factor of $1/n\pi$ as the image is *n* time point from the center of the window. To assess the impact of subtraction scheme on the resulting CBF data, all three subtractions schemes were implemented in this study and compared using the statistical F-test.

1.3.2 Motion correction

In any analysis performed across time the assumption is that the coordinates of a certain area in the image correspond to the same area in an image at any other time point. This assumption is becoming increasingly problematic with increasing time duration across which the images were acquired. This assumption is no longer valid in case of motion.

In the scanner, the subject is instructed to avoid from head movement. However, some types of motions are unavoidable, such as breathing. This type of motion is a periodic motion of which the effect is the appearance of “ghost” objects in the image. Such phenomenon is addressed in case those artifacts are visually detected in the image. It can be resolved by inspecting the frequency domain of the signal, and filtering out the frequency correspond to the frequency of the breathing. However, the standard procedure for cancelling the effect of motion is by aligning the images according to a certain reference. For that purpose, there are several algorithms that can be implemented, and as the goal is optimization, there are different approaches regarding the optimization procedure. Mathematically, those procedures are characterized by the cost function, of which its minima represent the optimal choice of parameters. The way the cost function is defined determines a certain choice of optimization.

The algorithm implemented in this study takes the image of the middle time point (considered here as time point zero) as a reference image. The procedure described below was done simultaneously towards the two time directions. For each volume, a search for the transformation parameters that minimize the cost function is performed. There are two search area parameters in each step, correspond to two different stages of the motion correction. A more coarse initial search with searching window of 8 mm isotropic. This is followed by a more refined search with searching window of 4 mm. The search in the first image adjacent to the zeroth image assumes a priori that no motion occurred. For the next image along the time series, the transformation found between the zeroth image and the first, is first applied on the zeroth image. Then the search procedure is identical as was described for the first volume. For the third volume, the second transformation is first applied on the zeroth volume and the procedure continues similarly for the rest of the volumes.

The optimization is done with respect to 7 motion parameters. Three rotations about the 3 Cartesian axes, 3 translations, one for each direction, and the displacement. The combination of the of these 7 parameters that minimize the cost function serves for the transformation and is plotted in figures 2.2 across the time points. Since the shape of the brain is preserved across the time point, the transformation is a rigid body transformation. Once the transformations were determined, an interpolation algorithm is performed for evaluating the new values of the voxels, values that are weighted by the new corrected locations of the old voxels.

There are sevens steps in total for trilinear interpolation [80]. Three steps to interpolate each of two collinear points (points p1234 and p5678) with respect to the point needed to be interpolated (point v), and a final last step to interpolate point v using points p1234 and p5678. Point v represents the corrected intensity in the voxel in the motion corrected image, whereas points p1-p8 are points of the image before the transformation being at the new locations assigned by the transformation. d1 is the ratio of the distance between v and p1234 and the distance between p1234 and p5678, where d2-d7 where determined similarly. The last step of the algorithm will be calculated by,

$$v = p1234d1 + p5678(1 - d1) \quad (32)$$

where,

$$p1234 = \square 12d2 + p34(1 - d2)$$
$$p5678 = p56d3 + p78(1 - d3) \quad (33)$$

where,

$$p12{=}p1d4{+}p2(1{-}d4)$$
$$p34{=}p3d5{+}p4(1{-}d5)$$
$$p56{=}p5d6{+}p6(1{-}d6)$$
$$p78{=}p7d7{+}p8(1{-}d7) \quad (34)$$

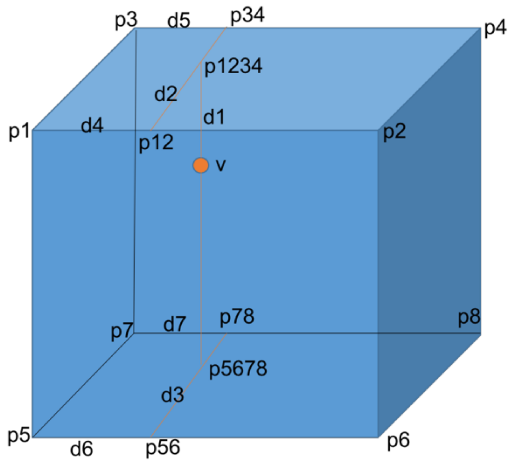

Figure 2.2. The trilinear algorithm is based on linear extrapolation assessment of the voxel intensity (point v) given the transformed point in its surrounding (points p)

1.3.3 Filtering

1.3.3.1 Spatial filtering

Spatial filtering is applied for increasing the signal to noise ratio (SNR). That is obtained by reassigning a new value to each voxel, which is a weighted average of the voxels within a predefined window surrounding the target voxel. In a simple local Gaussian filtering, the weights are defined to have a normalized Gaussian distribution in which the target voxel is its maxima. Although it reduces the amount of noise, it also damages the contrast by rendering the image more blur. Choosing a wider full width at half maximum (FWHM) will increase the blurring effect, whereas narrower FWHM will

reduce the averaging. The compromise often adapted is to set the FWHM to be of the order of magnitude as the voxel dimensions.

1.3.3.2 Physiological noise

the sampling rate of the perfusion time series is 8.6 s (2TR). Therefore, any noise component with period shorter than 7 s cannot be filtered from the data. Noise components of period longer than 7 s are associated with physiological changes that might affect the temporal SNR (tSNR). The respiratory and cardiac cycles are among the contributors for the physiological noise, although other factors have been pointed out as well. Those factors are related to hemodynamic metabolic fluctuations occurring mainly in gray matter areas, and are not fully understood [81]. It is for that reason that physiological noise is dominant in susceptibility weighted images, namely, it is TE dependent [82]. Therefore, physiological filter becomes more crucial in BOLD time course. However, no pulse sequence can prevent completely BOLD contamination as TE cannot be completely zero (in this study TE = 9.2 ms).

Assuming independent noise components σ_i, the total noise is,

$$\sigma = \sqrt{\sum_i \sigma_i^2}. \quad (35)$$

Here we distinguish between two noise components, σ_0 and σ_p which are the thermal Gaussian distributed noise and physiological noise, respectively. tSNR is defined as,

$$tSNR = \frac{S}{\sigma} \quad (36)$$

where *S* is the time averaged signal. Using those definitions, an expression for the physiological to thermal noise ratio can be obtained,

$$\frac{\sigma_P}{\sigma_0} = \sqrt{\left(\frac{SNR_0}{tSNR}\right)^2 - 1} \quad (37)$$

where SNR_0 is the special SNR. Thus, this ratio is scaled asymptotically with the SNR. That gives rise to the different nature of the physiological noise, consisting of physiological fluctuations which factorize the signal, rather than being an additional term as in the case with thermal noise. The noise factorization factor multiplying the signal is denoted by, which with the signal can be used to express the physiological noise,

$$\sigma_p = \lambda S. \quad (38)$$

Using the fact that,

$$SNR_0 = \frac{S}{\sigma_0}. \quad (39)$$

Rearranging equation [], the tSNR can be expressed in terms of the spatial SNR,

$$tSNR = \frac{SNR_0}{\sqrt{1+\lambda^2 SNR_0^2}}. \quad (40)$$

It can be deduced from this question that improvement in tSNR occurs only for small values of SNR_0. The constant, which can be extracted experimentally using this equation, determines the order of magnitude at which the spatial SNR will considered small. For example, for small values of, tSNR will still be approximately linear with SNR_0 and gains in spatial SNR will be translated into tSNR. However, for SNR_0 which is high enough, the tSNR approaches the constant $1/\lambda$. itself account for two terms contributing to the physiological,

$$\lambda = \sqrt{c_1^2 \Delta R_2^{*2} TE^2 + c_2^2}. \quad (41)$$

The constants c_i can be determined experimentally and R_2^* is spin the relaxation rate which is related to the susceptibility fluctuation. Hence, incensement in *TE* and with susceptibility fluctuation will farther limit the maximal tSNR available.

1.3.3.3 Physiological filtering

Filtering physiological noise is done by regressing out the physiological noise component from the signal of the raw images. For that purpose, the signal from the ventricles is spatially averaged and will be denoted as $v(t_i)$. the assumption is that measured time course signal at time point *i*, $m(t_i)$, can be decomposed into two components, a physiological component assumed to be identical to the ventricle signal, and a blood flow component, $f(t_i)$, namely the effect of the tagging. That is analogy to the way that a signal can be decomposed into a model component x_i and a noise component e_i where b_i are free parameters of the model,

$$y_i = x_i b_i + e_i. \quad (42)$$

The free parameters are determined upon minimization of the error. Given this assumption, the physiological noise can be regressed out by considering the following analogous equations,

$$m_i = v_i b_i + f_i \quad (43)$$

instead of being interested in the fitted model (namely the regressor x_i multiplied by the optimization free parameters), the "error" is of interest, as it represents the blood flow filtered from physiological noise.

1.3.4 ASL signal calibration

For quantification of the ASL signal, a measurement of the blood magnetization at equilibrium (m_b) is required (see theoretical section). In ASL techniques in which the spins in the ROI are not inverted during the control acquisitions, the control images can be used for computing m_b. In other cases, such as in this study, a separate pulse sequence is acquired on top of the ASL tag-control images, using a long TR. Several approaches exist for this evaluation. They can be classified into two main types: global value and voxelwise.

In the case of a global value approach, the assumption is that m_b changes very little between voxels containing blood flow and can be represented by a single global value. Estimating m_b voxelwise introduces another source of variability, thereby increasing the uncertainty in resultant CBF values. Although it may not improve the accuracy, this approach spatially stabilizes the CBF map [83]. For the order of magnitude of several Tesla, it can be farther assumed that T1 value of blood does not differ much from that of brain tissues, thereby justifying an average across the entire brain for obtaining an evaluation of m_b. That method can be implemented in case there is no anatomical information which allows more refined evaluation. However, difference T1 does vary quite significantly across the brain, manly in transition between between gray matter (GM), white matter (WM) and cerebral spinal fluid (CSF).

Therefore, other global methods consist on assessing the equilibrium magnetization by averaging only across brain area of type *i*, where *i* corresponds to GM, WM or CSF. By taking into account the T_2^* differences between the area used and that of

a blood, as well as the signal obtained from a proton density image, ρ_i, the equilibrium magnetization of the area *i* can be converted to m_b according to,

$$(44) \qquad m_b = \frac{\rho_i}{\rho_b} m_i e^{\left(\frac{1}{T_{2i}^*} - \frac{1}{T_{2b}^*}\right)TE}.$$

In the analysis, the control volumes were extracted from the time course and were served for the evaluation of m_0.

2. Methods

2.1 Experiment design

2.1.1 The motor task

The objective of this study was to detect changes in resting blood flow in motor areas, following and during learning of a motor task. The motor task used here is a sequential pinch force task (SPFT), in which a visual input has to be responded to by finger movements. The visual input is a moving bar (a reference bar, RB) that the subject sees on a screen. Simultaneously to the RB movement, the subject controls the position of another bar (FB) by exerting force on a pressure sensor device (figure 2.3). The subject has to match the position of the FB to the position of the RB by exerting the right amount of pressure.

There are two sequences involved in the experiment design, namely, two types of RB motion to which participants had to match the position of the FB. The simple sequence and the learning sequence. In the simple sequence the RB follows a pure sinusoidal motion, whereas in the learning sequence the RB performs a more complex movement, namely a superposition of several sinusoidal components. The simple sequence has two purposes. It is the sequence performed by the control group. Since following this sinusoidal pattern is an easy task to perform, no learning is expected to occur across the different sessions of the task after the initial familiarization with the device. This can be verified by observing a stable level of performance across days. Given that learning is associated only with improving performance, the control group can account for effects that are involved in the task, but not related to learning, such as the brain activation

evoked by the hand movements per se. The simple sequence is also used in the training group to localize the ROI of learning-related brain areas. The assumption is that areas associated with the finger movement during the simple sequence contain subareas that are responsible for learning during the learning sequence.

Two measures are used to evaluate performance on the task. One is the amplitude difference between reference bar and the force bar for estimating accuracy. A second measure is lag cross correlation from which the reaction time can be inferred. These metrics are not shown here as learning was assessed across days rather than as a function of performance.

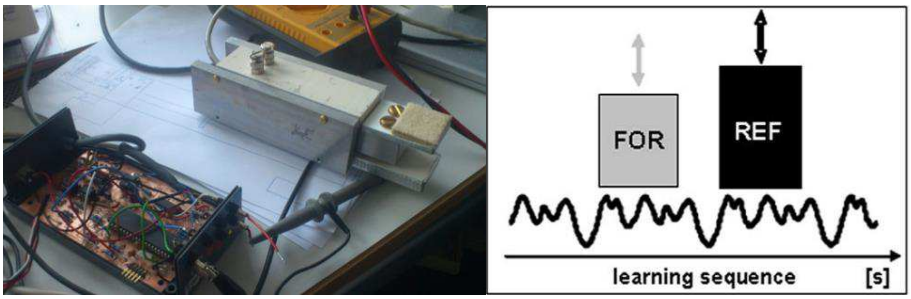

Figure 2.3. Left: the custom made pressure sensor used in the task. Right: a schematic diagram of the training sequence.

2.1.2 The learning timeline

The main part of the experiment timeline is 5 successive days of learning, in which the learning group performs one learning session per day of 20 minutes. On three of these learning days, an MRI acquisition is performed. Four days before the learning sessions, the participants are familiarized with the task by performing a simple sequence. An MRI acquisition is also performed on this day and the activation provoked by the simple task area is localized using a BOLD acquisition. BOLD is used during this initial session to ensure adequate SNR since BOLD is a more sensitive technique than ASL. As the main goal of this study is to detect changes in CBF, the CBF measurement of this pre-learning day is considered the baseline for the possible learning-induced changes. Twelve days following the last learning day, the participants performed once again the same task to account for

retention effects of the learning. Imaging was combined in the pre learning session (day 0), in the first, second and fifth days of learning as well as in the retention session. ASL was acquired right before and right after each learning session on learning and MRI days to look at short term effects of learning.

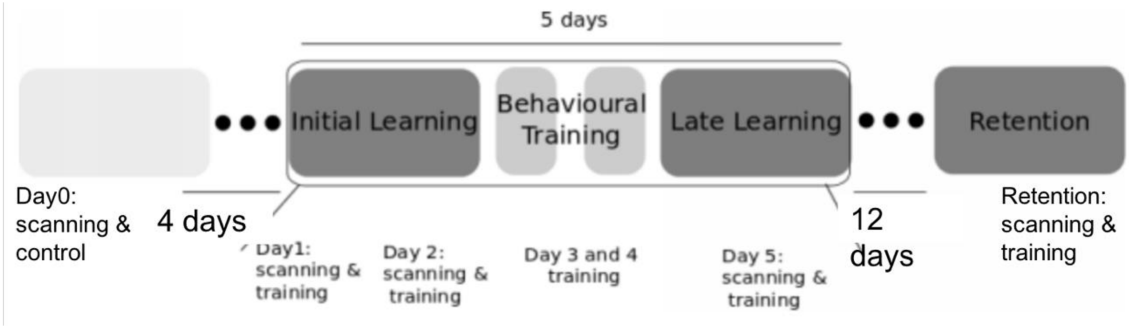

Figure 2.4. The experiment's time line.

2.2 Data acquisition

The anatomical data used in this project is a synthetic T1-w image created from two other images acquired using a magnetization prepared rapid gradient echo (MP2RAGE) pulse sequence [45]. This sequence was originally chosen to map absolute T1, rather than a T1-w image, but due to the need for dedicated processing tools to use this T1 maps, the T1-w image also generated using this sequence was used instead. This pulse sequence uses small flip angles, allowing to shorten the TR duration, and inversion. For each one of the two images a different inversion time (the duration between the inversion pulse and the image acquisition) is set, which allows reconstruction of T1-w image and quantitative T1 map. Both types of images are used for registration and extraction of ROI. The inversion times are T1/T2/TR/TE = 900/2750/5000/2.45 ms and the corresponding flip angles are a1/2 = $3^0/5^0$ with resolution of 0.7 mm isotropic.

The ASL raw data was acquired during resting state using a FAIR sequence and contained 41 interleaving volumes of tag and control. The last volume was discarded as only even number of volumes were considered. The pulse sequence parameters: TI1/TI2/TR/TE = 800/1500/4300/9.2 with flip angle a=90^0. Another similar acquisition was performed with the same parameters, except for having TR = 10000 ms, and 7 volumes.

This image was acquired to measure the fully recovered magnetization for ASL quantification. The long TR ensured that the magnetization will fully recover its longitudinal magnetization. The resolution of the ASL data was 3x3x3.5 mm.

Finally, the BOLD pulse sequence parameters, only used for the day 0 localization acquisition, were: TR/TE = 3500/20 ms with flip angle □ = 90^0. The BOLD time course contained 93 volumes with resolution of 1.5x1.5x1.5 mm.

In all the pulse described sequences, a 32-channel transmit/receive head coil was used on a Siemens 7T machine at the Max Planck Institute for Human Cognitive and Brain Sciences.

2.3 Demographics

Forty-six subjects were recruited for this study and 40 completed the entire study. Average age was 24.50±2.44. The control group consisted of 20 subject and the training group 20 subjects. Nine males were in the training group, and 10 males were in the control group. Only the training group was used in the results presented here.

2.4 Data processing

2.4.1 Pre registration steps

First, the ASL raw data was motion corrected using the FSL [87] tool MCFLIRT [84], according to the algorithm described in the theory section.

The brain extraction of each ASL time series involved several steps. First, the first volume of the time series was brain extracted. Then, a threshold was used for the binarization of the image, for excluding voxels that contain background noise. As the differences in the intensities between brain areas and the background is several orders of magnitude, the threshold could be set such that only negligible part of the brain would be lost. Lastly, all the volumes were multiplied by the mask, thereby leaving only brain in the multiplication image. This method of brain extraction for a time series has the advantage of maintaining a similar external brain contour in the end of this process for each of the volumes.

A Gaussian filter of FWHM = 4 mm was chosen and was applied on the raw data (since the ASL data processing consists entirely on linear operations, the Gaussian filtering may be applied at any step). This FWHM was chosen to preserve as much as possible anatomical boundaries while still increasing SNR.

For the physiological filter the T1-w image was brain extracted and registered to the ASL native space. The functional intensity threshold of the brain extraction was 0.35. The CSF was then extracted from the T1-w image in qT1 space using a K-means algorithm with 3 classes. The matrix produced from the registration of the anatomical image to the ASL native space was used for registering the segmented CSF to the ASL native space. To exclude CSF outside the ventricles, a template of the ventricles from an MNI atlas was also registered to the ASL native space. The registration was done using a similar strategy, where an anatomical image in the same space as the atlas, the MNI152 space, was registered to the ASL space. The matrix used for this registration was then used to transform the ventricle template to the ASL native space. A liberal threshold was implemented on the registered ventricle template for ensuring that the segmented ventricle of each subject will be included within the ventricle template. Then a conservative threshold was used for the binarization of the segmented ventricles.

Before subtraction, the volumes were inspected visually to ensure that corrupted data would be excluded. In a few cases, the data were corrupted during the file transfers, requiring the retransferring of data from the server at the Max Planck institute. The ASL data were pair-wise subtracted for all the subject. For the scan from day 0, we used also surround and sinc subtraction for statistical comparison using F-test. After subtractions, the perfusion data were time averaged for all the time points, whereas on day 0, the data were also spatially averaged over GM for the statistical analysis.

To obtain the CBF maps, the average PWI images were used as the input into the oxford command line in FSL. The model for quantification is described in the theory section. The selected inversion efficiency was 0.98, a typical value for pASL. The T_2^* of blood was set to 37.5 ms, T_1 of blood was set to 2.23 s, and T_1 of CSF was set to 4.4 s.

For the purpose of the calculation before registration, perfusion data were truncated, for removing slices containing artifacts in the lower and upper parts of the image. After truncation, 9 out of the 15 slices were kept, containing the ROI. A similar procedure was done for data in MNI152 space (see below), leaving 41 out of the original 91 slices in the image.

Most of the ASL data processing was done on FSL in a MATLAB programming environment.

2.4.2 Registration

Registration is a process in which an image is modified by a transformation to match the coordinate space of another, typically a reference, image. This procedure is often needed when two are more images of different types, of different subjects or acquired at different times must be compared or combined. To be able to do any operation or to refer to certain coordinates of one image based on information that exists in the other image (such as anatomical information), these two images have to be in the same coordinate space. In other words, they have to match, in the sense that the coordinates of a certain location in the brain will be the same in both imagesMost of the analysis described so far was performed in the same coordinates as those of the images received from the scanner, with the exception of the anatomical needed for the physiological noise. In this case, since the ventricles cannot be extracted from the ASL data, as it does not contain clear anatomical information, an anatomical image was registered to the ASL space. For performing ROI analysis however, the CBF maps have to be registered to a common template in a space where the ROI can be extracted.

The registration of the CBF maps (and SNR maps) was done in two steps. First, the ASL data was registered to quantitative T1 space (qT1), using mappings constructed at the Max Planck institution in Leipzig, per subject and per day, using sinc interpolation. qT1 refers to a subject-specific template, constructed by the co-registration of the five anatomical images from each participant. The anatomical data acquired per subject and day allowed the construction of mappings that transformed each one on the ASL data at

the qT1 space to the space of the common template. That was done by registering the anatomical image first, and then applied the matrix of this registration on the ASL data correspond to the anatomical image.

The regions of interest, which were M1 and SMA, were extracted using the Oxford-Harvard brain atlas. The template in the common space was the MNI152 with 2 mm isotropic resolution. All the registration performed with FSL were linear registrations with 12 degrees of freedom and trilinear interpolation. The registration from ASL native space to qT1 was done in MIPAV software and is a non-linear registration with sinc interpolation using the ANTS tool.

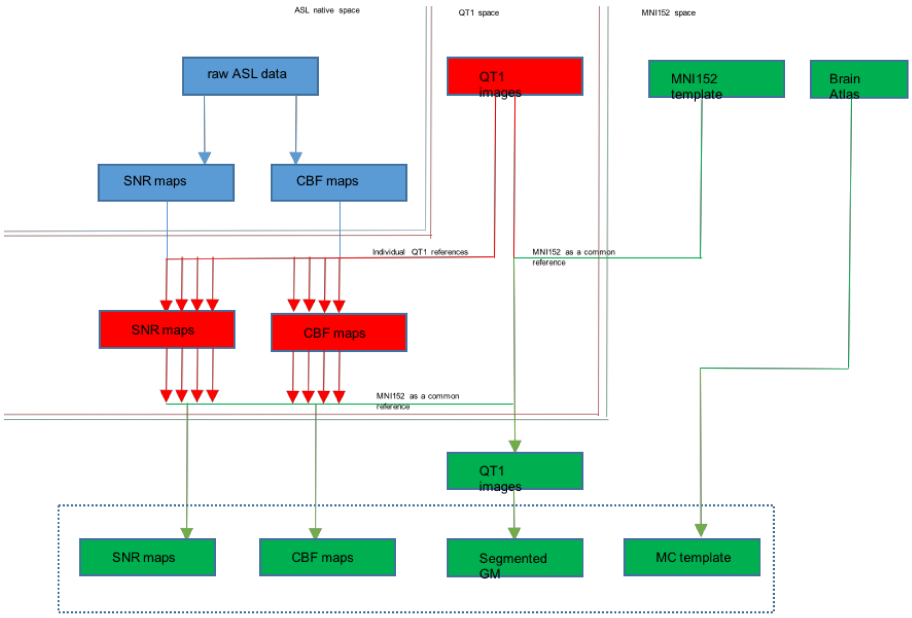

Figure 2.5. Flowchart describing the registration process done in FSL.

2.4.3 Localization

The term localization refers to the extraction of CBF values from areas from where there is an expectation to see a change across time points. This extraction can be performed on the ground of main three strategies.

2.4.3.1 Anatomical region of interest

As was discussed in the introduction, the main region of interest covers M1. In this study, the SMA was also be extracted for calculation. These two areas were masked in the MNI152 common space after being extracted from Oxford-Harvard brain atlas. The brain atlas assigns integer value of intensity to each different brain area in the parcellation.

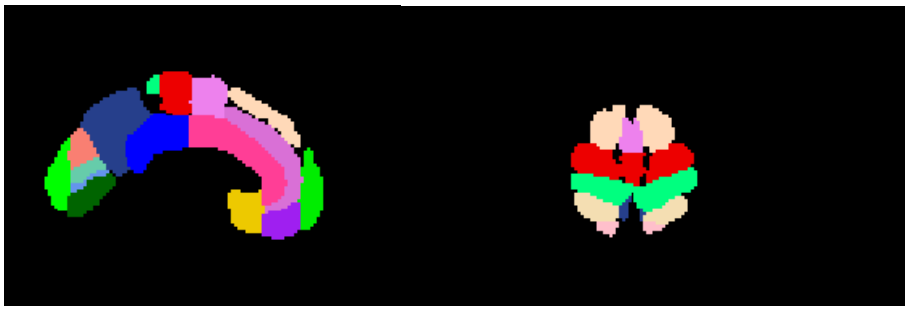

Figure 2.6. Left: a sagittal view of the Oxford-Harvard parcellation. M1 is in red, and SMA is in pink. Right: an axial view of the atlas. The M1 extends across the angular gyrus, whereas the SMA is mainly at more medial location.

A MATLAB script was used to create 2 images in which only the area desired was included, one image for each area, and their area was restricted to the left hemisphere since the task was performed with the right hand. Multiplying each one of these mask with the CBF maps, allowed to average only over these areas. However, these areas were not specific enough, as the changes are expected to come from a specific area of the M1, namely the area associated with finger movements. Therefore, a more refined localization was implemented.

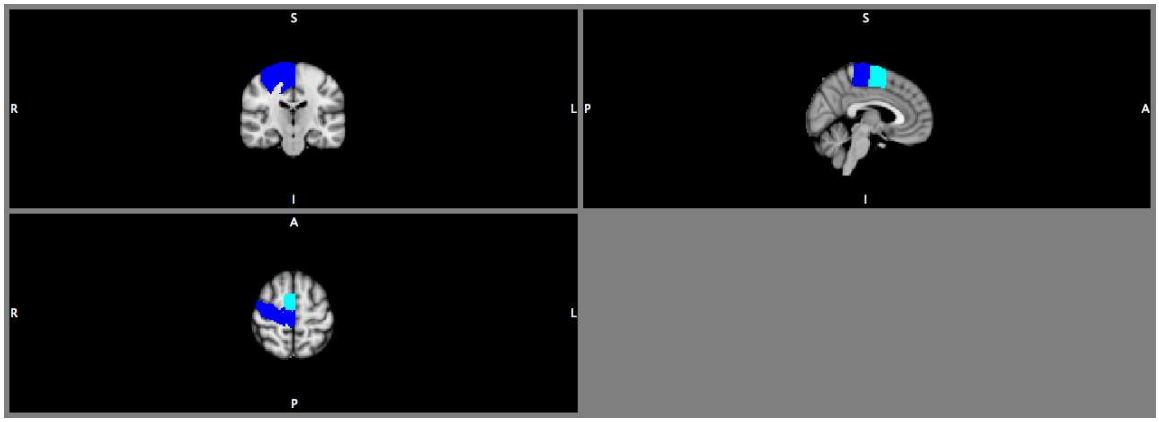

Figure 2.7 the Oxford-Harvard templates for the M1 (blue) and the SMA (light blue) laid-out on the MNI152 brain template.

2.4.3.2 Functionally-defined M1 region of interest

Although CBF was measured before and after learning rather than during learning, the expectation is that learning-induced changes will occur mainly in regions activated while the subjects performs similar finger movements as they perform during learning, since these are the areas involved in the task. Plasticity can occur with the repetitive use of neurons, and hence the association between task-related areas of activation and CBF changes. This assumption allows to be more specific regarding the region of interest, as there are areas in M1 that a priori can be considered as non-task-related, namely, areas associated with other body parts.

The task-related ROI was determined using the BOLD response to the simple sequence performed on day 0. The BOLD response is obtained by acquiring a time series of images that are sensitive mainly to the deoxyhemoglobin level in blood. Areas of activation are localized by exploiting the fact that there is an hemodynamic response in areas of activation. This hemodynamic response means that these areas are flooded with oxygenated blood, creating a signal difference between baseline and activation. Thus the BOLD time series acquisition should include a baseline period, namely when the subjects do not move their figures, and an activation period, namely when the subject engage in performing the control sequence of the task.

For preparing the functionally-defined M1 ROI based on the BOLD response, the

FEAT software tool of FSL was used. A high pass filter was applied to the BOLD time course to filter out signal component with period longer than 150 s. The MCFLIRT tool of FSL software [15] was then used for motion correction and a 4 mm FMHW Gaussian filter was used for spatial smoothing. The chosen kernel corresponds to the smoothing kernel used also with the ASL data. A general linear model (GLM) model with a boxcar regressor (a predictor for the activation component of the signal) corresponding to the rest-activation period of the task was used. a graphical representation of the regressor is shown in figure 2.8.

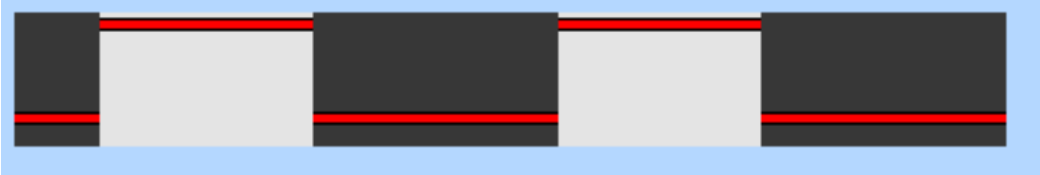

Figure 2.8. Regressor's graphical representation. The height of the red line and the and the brightness of the background represent the value of the regressor

A Z-test was performed to determine significance level of activation using threshold of z = 2.3. Cluster thresholding was selected for defining contiguous areas and then determining by a statistical test whether they consist a cluster, using threshold of p = 0.05.

2.4.3.3 Localization by temporal signal to noise ratio

The last localization method was based on the exclusion of voxels where the tSNR was not high enough to provide a reliable measure of the perfusion signal. For that purpose, the perfusion time course is considered, namely, after the subtraction of the raw ASL data and before time averaging. Since the signal consists of only base, a time average is an indication to the signal, whereas the standard deviation is an indication for the noise.

Reproducibility was defined as the mean coefficient of variability across subjects of the mean CBF in M1 between the day 0 scan and the pre-training scan of training day 1.

Statistics on the CBF data was calculated using IBM SPSS for Windows, version 23 (Armok, NY, USA: BM Corp).

Chapter 3 - Results

1. Data processing

1.1 Subtractions

Three types of subtraction were performed on the ASL raw data: pair-wise subtraction, surround subtraction and sinc subtraction. The time-averaged PWI of a random sample of 3 subjects are shown in figure 3.1. The cross-subject average signal for day 0 were 7.70±1.75, 8.08±2.03 and 9.18±2.31 a.u. using the pair-wise, surround and sinc subtractions respectively. These subtraction schemes were found to be significantly different (F-test; P=0.0015). As the pairwise subtraction introduced the lowest variability showed by the lower standard deviation across subjects, it was used for later processing.

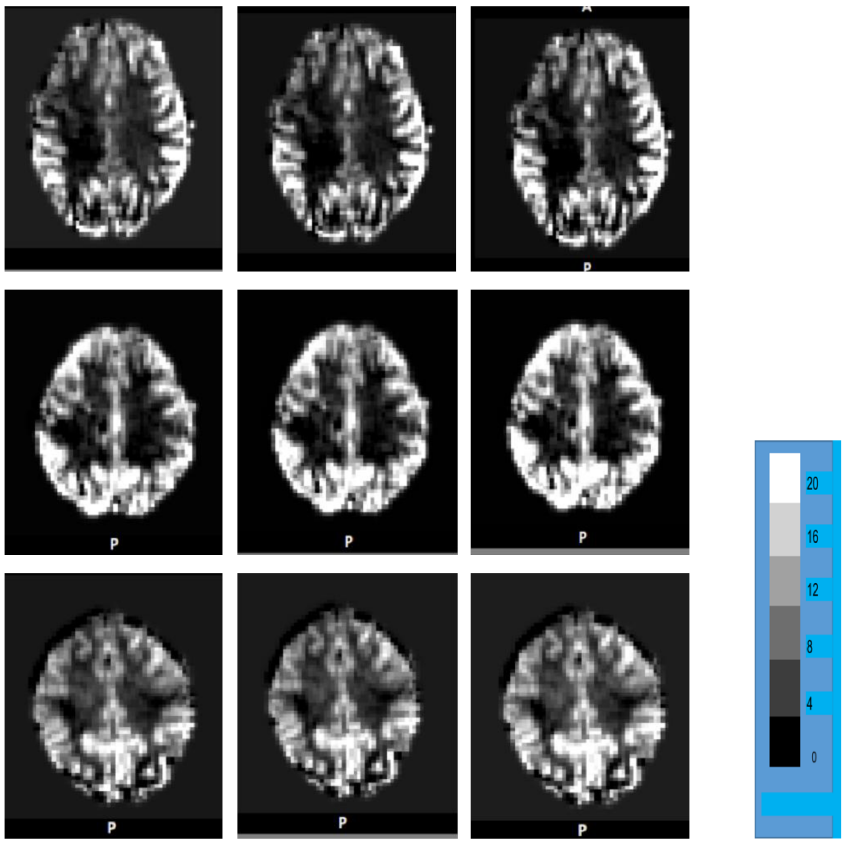

Figure 3.1. Perfusion weighted images. The columns left to right: pair-wise subtraction, surround subtraction and since subtraction. Different rows correspond to different subjects.

1.2 Motion correction

The motion correction optimized parameters are plotted for in figure 3.2 for a random subject. No severe motion artifacts were observed across all the subjects. This was quantitatively confirmed by comparing the corrected time series to the original. The average motion effect was $1.1 \cdot 10^{-3} \pm 0.4 \cdot 10^{-3}$ and thus the effect of the motion correction was limited. In the example shown in figure 3.2 a relatively significant translation occurred slightly after the 30th volume.

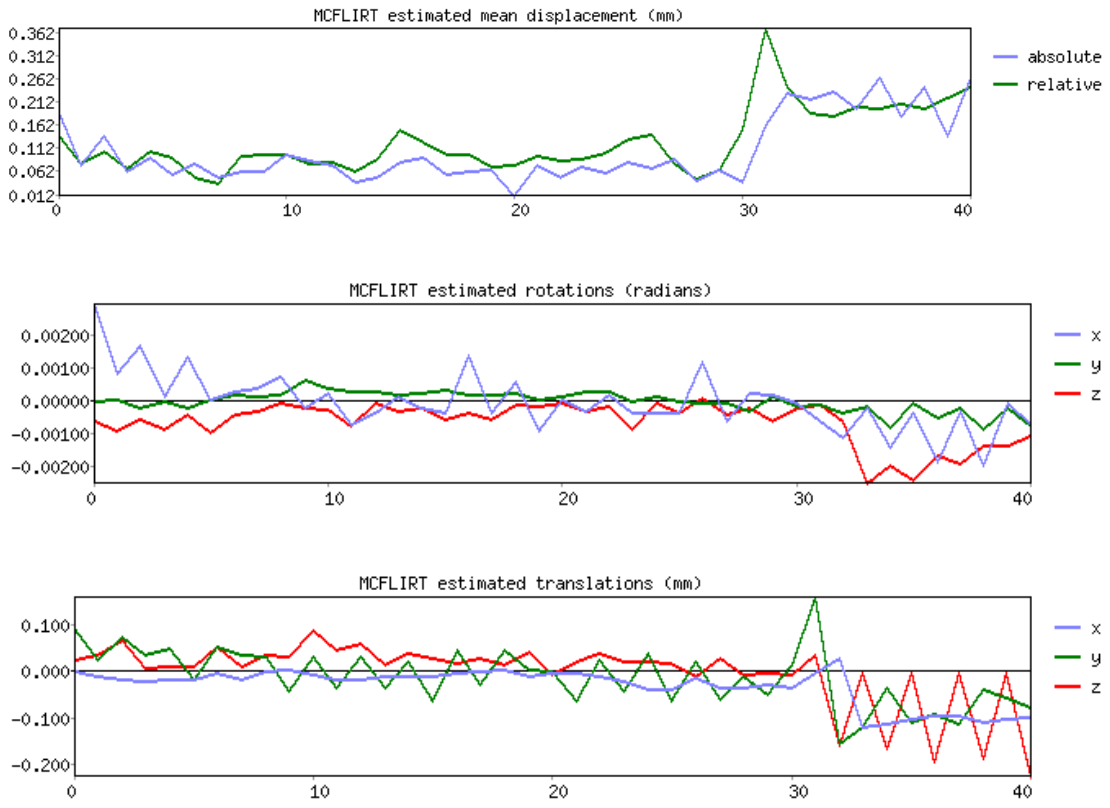

Figure 3.2. The different motion parameters as a function of the volume number.

1.3 Brain extraction

Brain extraction of ASL data is more challenging than for standard BOLD data as the TE typically used is shorter and therefore gives rise to a bright scalp signal. An example of successful brain extraction in a representative subject is shown in figure 3.3. The main non-brain element is the scalp. The removal of the scalp was performed successfully for

all subjects. The inclusion or exclusion of brain tissue in this process is determined by a functional intensity threshold that may range between 0-1. Here it was set to 0.5 uniformly through all subjects.

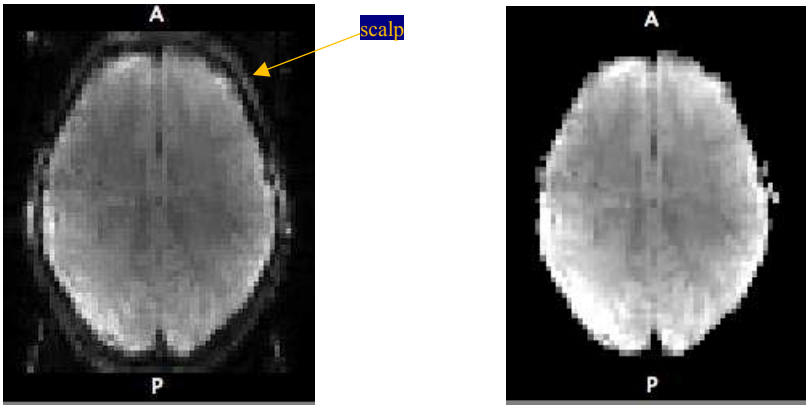

Figure 3.3. Brain extraction. Left: before brain extraction. Right: after brain extraction.

1.4 Filtering

The effect of the spatial filter is shown in figure 3.4 for a random subject. The filter resulted in lowered extreme values and decrease in the signal averaged across all brain for non-zero voxels. The whole-brain average (non-zero voxels) across subjects for day 0 was 7.30±1.77 a.u. before filtering and 3.67±0.96 a.u. after filtering. However, the total intensity was preserved.

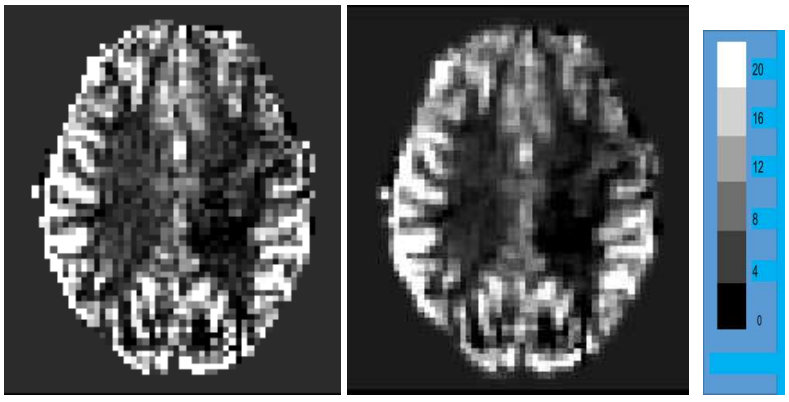

Figure 3.4. Spatial Gaussian filtering. Left: Before filtering. Right: after filtering.

The procedure performed on the anatomical image prior the segmentation of the CSF, is shown in figure 3.5.

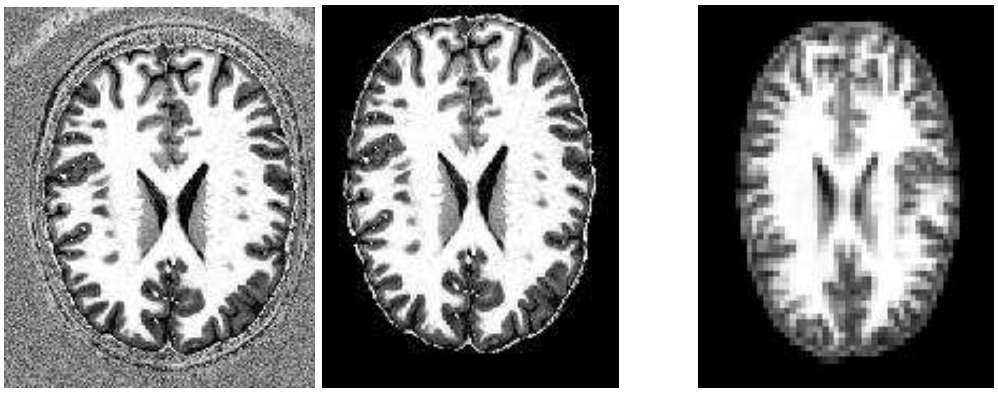

Figure 3.5. Left to right: the T1-w image before and after brain extraction. The registered T1-W image in ASL native space.

Initial CSF segmentation yielded an image containing both the ventricles and the sub-arachnoid space CSF (Figure 3.6). The ventricles area was successfully extracted from this image using the ventricle template from the MNI152 atlas. This extraction could not however precisely preserve the shape of the ventricles. The threshold was set such that voxels outside of the ventricles would be completely excluded, causing also a loss of voxels within the ventricles. However, the threshold was set such that for all subjects there was a sufficient number of voxels to average.

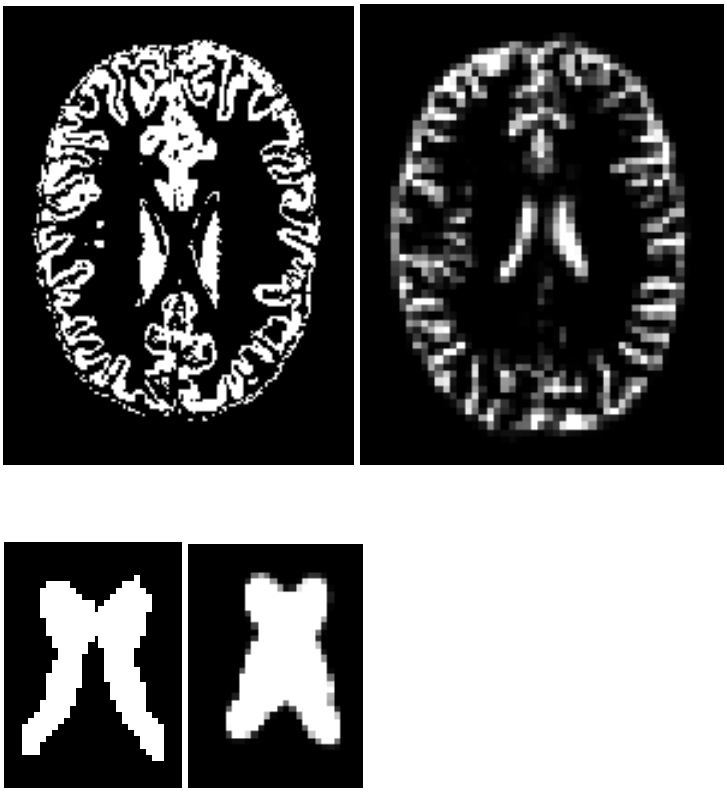

Figure 3.6. Top: the segmented CSF in qt1 space (left) and in ASL native space (right). Middle: the ventricle template in MNI152 space (left) and in ASL space (right). Bottom: the ventricles mask in the ASL space.

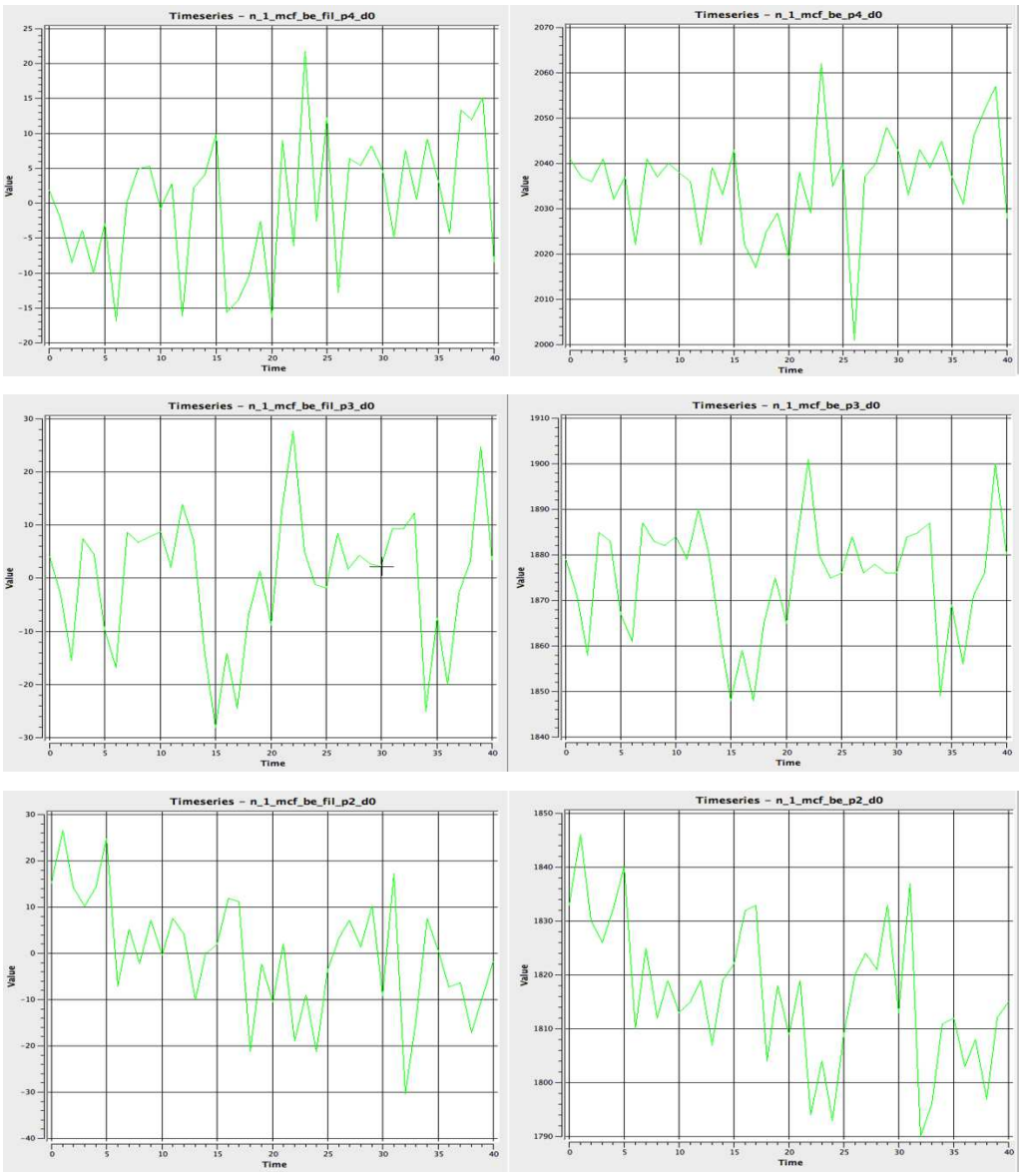

Figure 3.7. An ASL raw data time course of a randomly selected voxel of three different subject. Left column: after physiological filtering, right column: before physiological filtering.

The signal from the ventricles was then regressed out of the ASL signal (Figure 3.7). The effect of the tagging can be seen across the time courses. Odd time points are tag, and thus tend to be minima, whereas the even tend to be maxima. The physiological filter modestly modified the time course. In some cases, it enhanced the effect of the tagging, as can be seen between time points 20-25 in the upper row (Figure 3.7). Once averaged over brain areas and across subjects however, the removal of the signal from the

ventricles from the ASL signal led to a limited improvement of the flow signal. The average PWI signal in grey matter, averaged across all subject for the day 0 acquisition was 7.70±1.75 a.u. after filtering, and 7.96±2.03 before filtering. The effect of the filter was similar across all brain areas used in this project. For most of the voxels the effect was on the order of 0.1-0.2%.

2. Quantification

2.1 Cerebral blood flow quantification

Two methods of calibration were used for the quantification of the ASL signal, a "single method", based on a single representative m_0 averaged over CSF, and a voxel-wise method. The CBF maps from these two methods for a random subject are shown in Figure 3.8. The average CBF in grey matter, averaged across subject for the day 0 scan was 35.60±6.96 ml/100gr/min and 42.46±14.78 ml/100gr/min for the single and voxel-wise methods respectively. While the intensity distribution of the two images were similar, the values obtained with the voxel-wise method were more consistent with the expected physiological range [37].

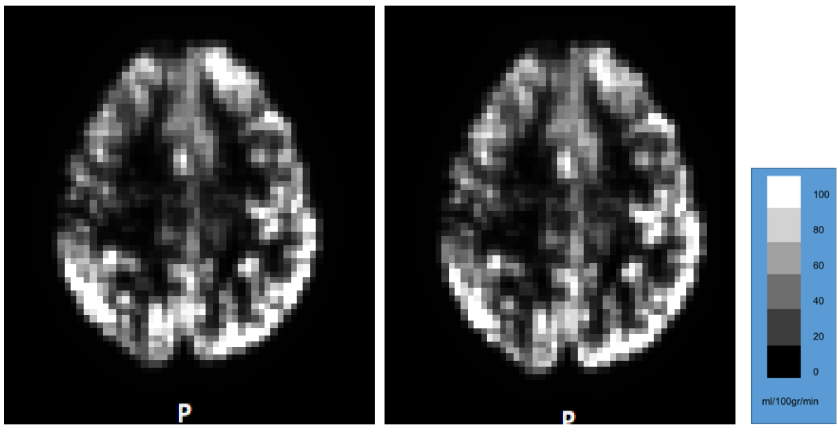

Figure 3.8. CBF map for a randomly selected subject. Left: using single value method, right: using the voxel-wise method.

2.2 Cerebral blood flow registration

After registration to MNI152 space, the average CBF across subject in GM, M1, SMA and the functionally localized area for day 0 was 42.28±6.96, 29.23±6.27, 30.44±8.84 and 18.32±8.58 ml/100gr/min respectively.

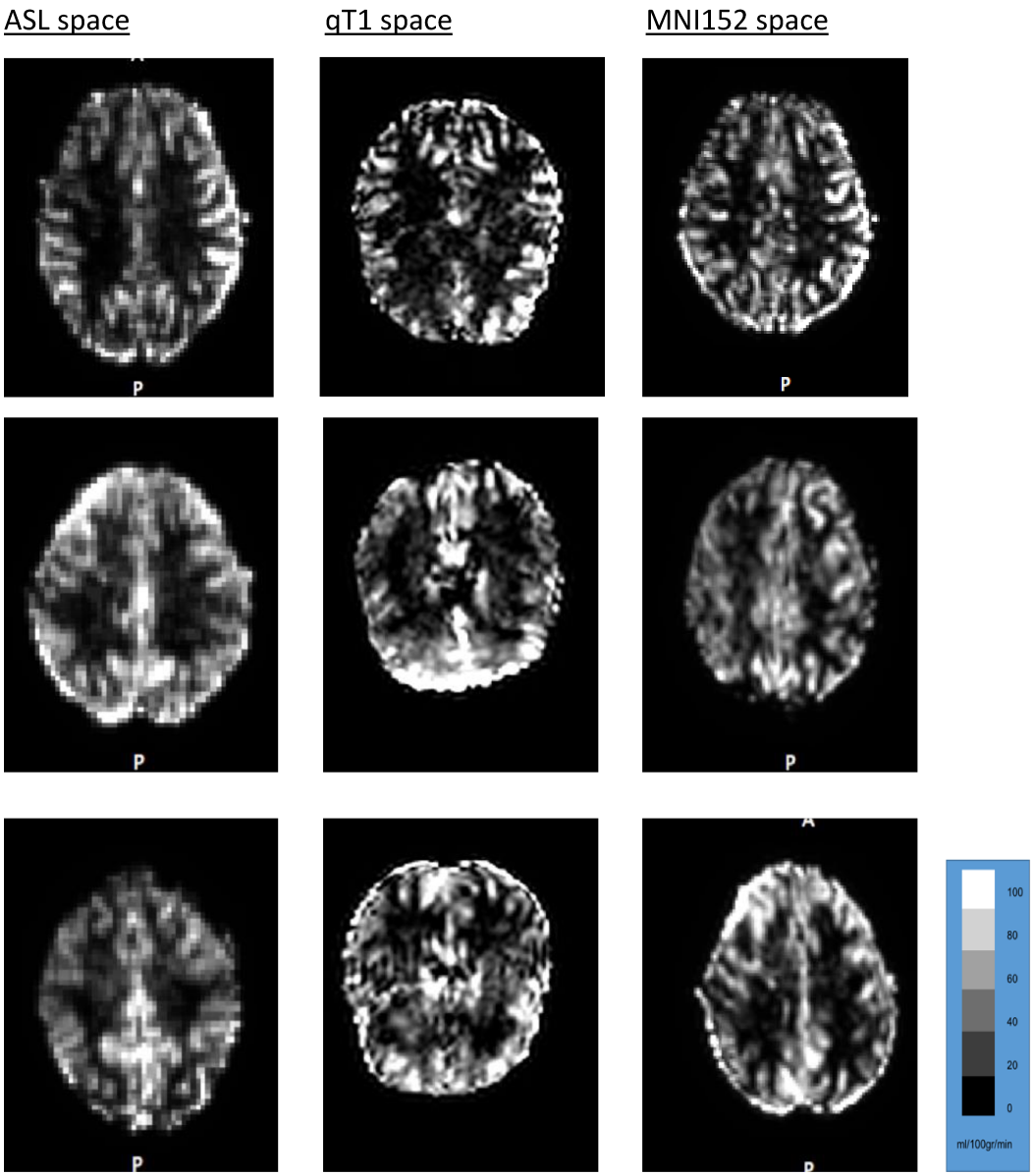

Figure 3.9. CBF map for randomly selected subjects in the different spaces. Left to right: ASL, qT1 and MNI152 space.

2.3 Temporal signal to noise ratio

The averaged tSNR in GM across all subjects in day was 0.73±0.18. The physiological filter did not improve the tSNR, as the value without filtering the ASL time course was 0.74±0.17. Mean tSNR on day 0 in M1, SNA and functionally-defined M1, averaged across subjects is given in figure 3.10. Figure 3.11 shows a tSNR map for a random subject, with no threshold, and with thresholds of 0.3 and 0.6. As the threshold was increased the similarity between the averaged values with and without the physiological filtering remained the same. The average SNR with threshold of 0.6 was 1.03±0.14. As seen in Figure 3.10, thresholding reduced predominantly white matter voxels, though the higher threshold yielded a significant loss in low SNR grey matter voxels.

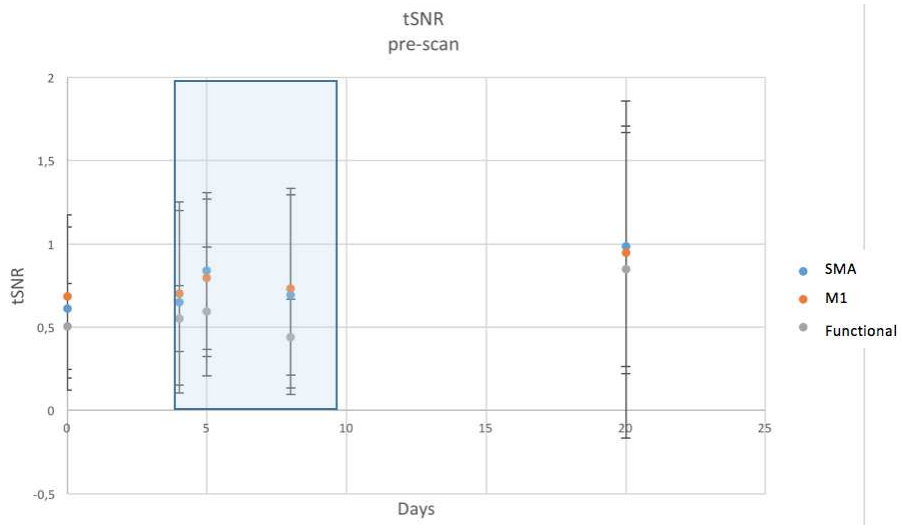

Figure 3.10. tSNR as a function of time for the SMA, M1 and functional M1. The shaded area represents the learning period.

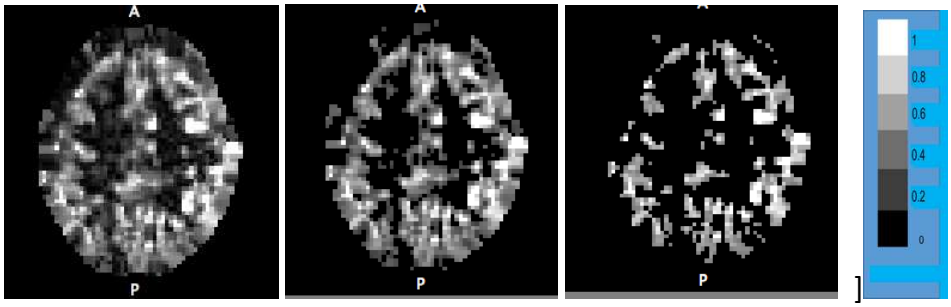

Figure 3.11 SNR maps for non-threshold, and 0.3 and 0.6 thresholds

3. Cerebral blood flow assessment on the regions of interests

3.1 Reproducibility

Between day 0 and the first training session no CBF change is expected, and thus those two scans can serve to evaluate the reproducibility. The coefficient of variability across subjects for day 0 versus day was found to be 0.16,0.20 and 0.25 for the M1, SMA and GM respectively. Calculating reproducibility using intraclass correlation (ICC), we found values of 0.57, 0.67 and 0.62 for the M1, SMA and GM respectively.

3.2 Mean Cerebral blood flow

In order to show task-dependent short term and longer term learning, the average M1 and SMA CBF values from anatomically-defined ROIs for all ASL acquisitions are shown in Figure 3.12 and 3.13 respectively.

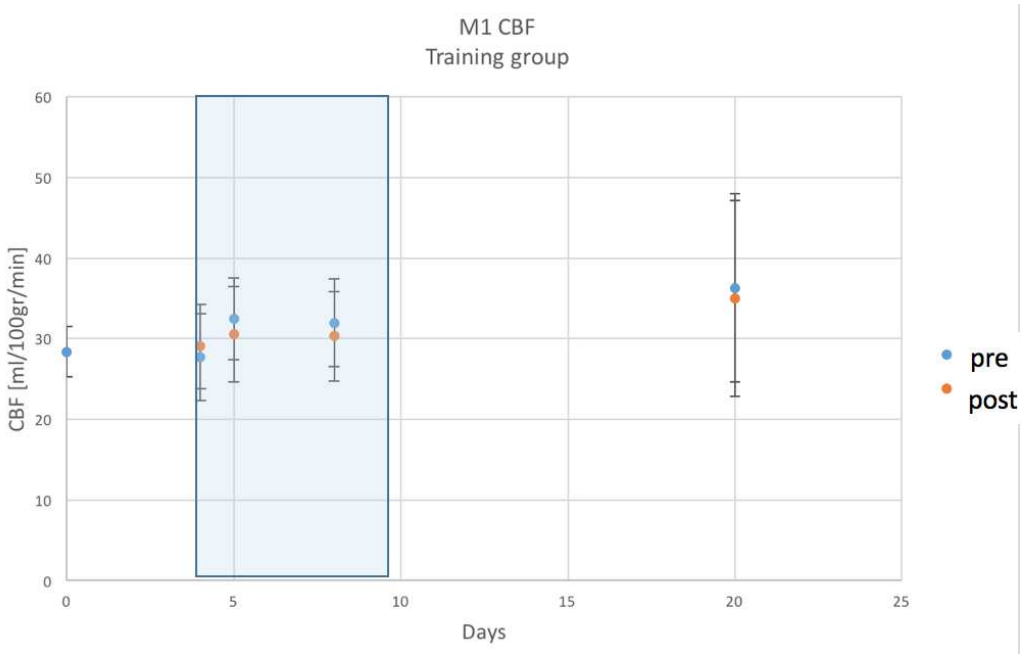

Figure 3.12. Averaged CBF over the M1 as a function of time for pre (orange) and post (blue) scans.

The same plot is shown in figure 3.13 for the SMA

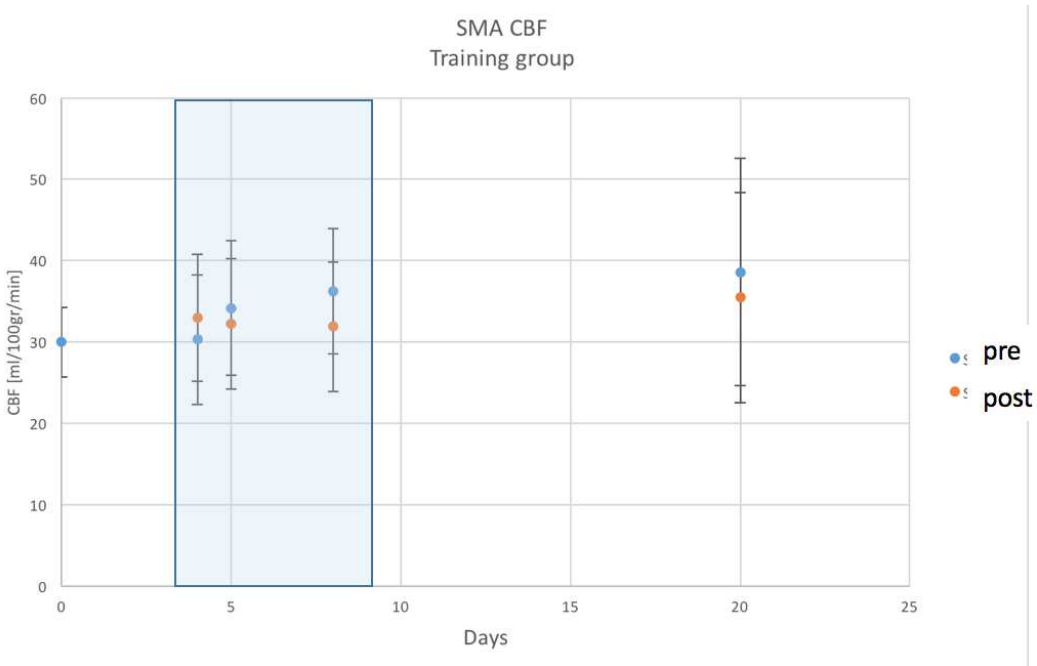

Figure 3.13. Averaged CBF over the SMA as a function of time for pre (orange) and post (blue) scans.

Mean CBF in ROI defined by using the functional localizer is shown in Figure 3.14. Only the training group was considered in defining this ROI.

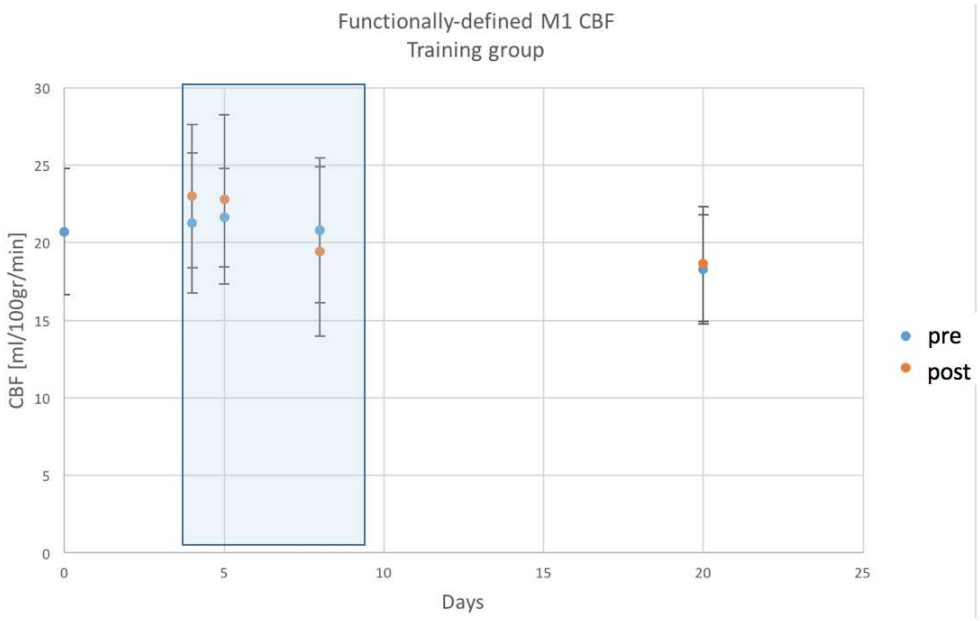

Figure 3.14. Averaged CBF over the functionally-defined M1 as a function of time for pre (orange) and post (blue) scans.

M1	P value	SMA	P value	Functional M1	P value
pre	0.695	pre	0.257	pre	0.600
post	0.559	post	0.545	post	0.666

Table 3.1. P-values evaluating the significance in changes across the training days.

	P values			
Day	4	5	8	20
M1	0.387	0.360	0.544	0.530
SMA	0.261	0.278	0.111	0.054
Functional M1	0.347	0.541	0.377	0.789

Table 3.2. P values evaluating the significance of changes between the pre and the post.

The CBF differences in the functionally defined ROI of the pre-scans in the 4 time points with respect to the individual baseline (day 0) was calculated and then averaged across subjects. The results are summarized in table 3.3.

Pre scan	Day 1 – day 0	Day 2 – day 0	Day 5 – day 0	Retention – day 0
Mean CBF	-0.61	2.08	3.43	1.80
STD	10.84	9.86	6.47	9.32
P value	0.964	0.596	0.973	0.361

Table 3.3. Differences between pre scans and the baseline scan on day 0 for each one of the training sessions where scanning took place and retention day.

Finally, the mean CBF was calculated at the M1 and SMA, using a GM mask for excluding voxels of WM region. Averaged values across subjects as a function of time are given in figure 3.15

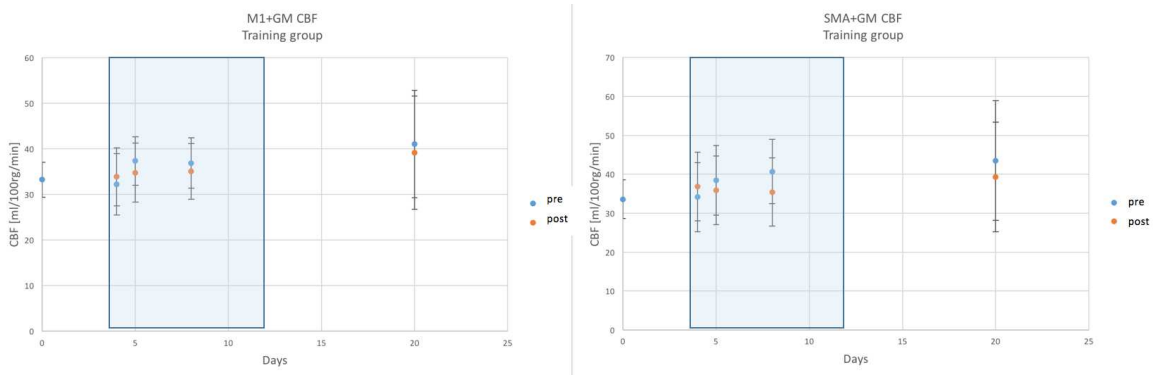

Figure 3.15. Left: Averaged CBF over region included within the M1 and GM as a function of time for pre (orange) and post (blue) scans. Right: Averaged CBF over region included within the SMA and GM as a function of time for pre (orange) and post (blue) scans.

Chapter 4 - Discussion

1. Data processing

1.1 Subtractions

Three different subtraction schemes were tested. As described by Liu *et al*, the effect of the subtraction is equivalent to a time-domain filter, where pair-wise subtraction is a low-pass step function filter. The data presented here shows a bias towards higher CBF values when using sinc subtraction. It is not clear, however, what is the source of the bias towards higher values in surround and sinc subtractions. Nevertheless, the differences were minor and probably would not have a large impact on the end learning results.

1.2 Motion correction and brain extraction

Motion correction was the first operation done on the ASL raw data. Since the brain extraction was based on multiplication of all the volumes in the ASL time course with a brain mask of the first volume, that fact enabled the optimization of the brain extraction, where the alignment of the volumes is highly important. Moreover, the presence of a scalp in the motion correction may lead to better results, as the high contrast of the scalp provides a reference line, thereby rendering the search process in the motion correction algorithm more stable. Brain extraction serves in cleaning the noise from the image background and reducing edges artifacts. An alternative approach for brain extracting of a time course, is brain extraction volume by volume. Comparison between the 2 approaches yielded better results when masking the first volume, as less edges artifacts were observed.

Due to the small volume of the 32-channel coil on the 7T machine, motion is typically modest at 7T. Additionally, as only experienced MR participants were allowed to participate in 7T experiment, data from this machine has been found to be small in most studies from the Max Planck Institute. This was reflected in our data and the motion in all

subjects found to be small. Therefore, this also indicates that the low SNR of our data cannot be attributed to movement.

1.3 Filtering

The objective of the spatial filtering was to increase SNR, while maintaining the internal structures, mainly that of the gyri. The chosen FWHM was larger than the voxel dimension (4 mm in comparison to 3 mm), but smaller than the typical kernel size used in fMRI studies (2x the voxel size). This was done to preserve cortical structure, notably the in the area of the motor cortex, but was larger than the voxel size to gain SNR.

For the purpose of the physiological filter the ventricle region had to be extracted from the ASL data, using anatomical information. The rationale for the exclusion of other CSF area besides the ventricles relates to the fact that the spatial resolution was not high enough to ensure that partial volume effects due to nearby grey matter would be minimal. Contaminating the ASL signal from CSF with real CBF signal will undermine the working principle of the filter. Fitting the MNI152 ventricle template to the individual registered ventricles in ASL space was problematic due to the variability in the shapes of ventricles of different subjects. The registration used here could not account in this case for that variability, since the individual reference image of the ASL data does not contain anatomical information. Also, linear registration was used and we were thus unable to locally deform the image. To compensate for this, a low threshold was used when binarizing the registered MNI152 ventricle template. Since it was then multiplied by the CSF mask, it was unimportant if it contained areas outside the ventricles of an individual subject. Future implementations of this method could use the individual anatomical information rather than the MNI152 to better define the ROI.

One of the effects of the filtering procedure on the ASL time course was the cancellation of the baseline component. The was expected, as the signal emerging from the ventricles contains a similar baseline component to any other brain area. In fact, this baseline is partly related to the noise to be removed. However, the physiological noise is associated with changes in this baseline. This should not influence the flow-dependent

component however, as this flow-dependent signal consists of the difference between time points. The physiological filter also changed the relative intensities between time points, but these changes were minors. Since the effect of the filter is mainly on the baseline rather than on the effect of the tag and control, it can be concluded that the signal from the ventricles is not significantly affected by changing physiological parameters, and thus has limited ability to filter out physiological noise. It could be that other brain areas would be better suited for filtering out noise terms from the CBF. One possibility is the white matter. There is reason to believe that white matter is more representative of the physiological fluctuations and may serve as a better regressor. However, although CBF in WM is low, it is not zero, and thereby by may lead to a loss in perfusion signal. Future studies could assess the relative merits of CSF and WM signal for noise correction.

2. Quantification

CBF values in the brain showed the expected distribution, namely higher values in GM area in comparison with WM. Moreover, for GM area, the values were in the physiological range, although below some values previously found for a similar population. The lower values may be the result of non-optimized GM extraction in this study. The GM mask did not perfectly cover the circumvolutions of the cerebral cortex, leading to the partial volume inclusion of CSF inside sulci and WM.

Another aspect of the processing which may have led to sub-optimal CBF quantification was the measurement of the fully relaxed magnetization M0. Two methods of calibration were tested, using a single value for M0 and a voxel-wise M0 methods. The single value method led to CBF values that were out of the expected physiological range, and thus was not used further. The voxel-wise method, on the other hand, yielded values within the expected physiological range. The reason for the overestimation of the CBF value using the single value method was underestimation of M0 of CSF. On the other hand, the voxel-wise method does not depend on an estimation of a single value, but is

based on local information. The draw back in this case, is the additional spatial variability introduced into the CBF calculation. This factor was not found to dominate in our CBF estimation and the voxel-wise method provided CBF maps with more physiological values.

Finally, the registration of the CBF data to the common MNI152 space was not optimal. As can be seen in figure 3.9, some of the geometrical characteristics of the image, namely the shape of the brain, and cerebral cortex reflected from the CBF map, were not well aligned with the MNI152 template. This was problematic for quantification within anatomically-defined ROI from the Oxford-Harvard atlas (M1 and SMA) since these ROIs may not always be well aligned with GM voxels. This problem was less present in the case of the GM ROI, as this ROI was defined using individual anatomy rather than an atlas in template space. In the case of these anatomically-defined ROIs, this mis-alignment due to non-optimized registration therefore led to a lower mean SNR.

3. Temporal signal to noise ratio

ASL is known to be a low SNR technique, and the SNR on a head-only 7T scanner has typically been found to be lower than at the more commonly used 3T field strength. This is both due to field inhomogeneities and because the coil does not cover the neck area, making it necessary to use older and more inefficient ASL techniques such as FAIR. Although ASL is a low SNR technique, tSNR maps can be used to filter out voxels that deteriorate the overall image SNR. As expected, the voxels with higher SNR are located in areas of higher CBF values, which are also typically areas of interest. Moreover, the standard deviation across subjects decreased as the SNR increased with higher tSNR threshold. Thus, preserving only high tSNR voxels contributes to the stability of the data. While this technique may in general be beneficial, it was somewhat limited in this case due to the lower SNR nature of the 7T data used. The threshold could not be set too high, as the number of voxels reduces rapidly with threshold, and may not cover the ROI, or be sufficient for properly averaging.

4. Cerebral blood flow assessment over regions of interest

While the ROI CBF comparisons performed yielded non-significant results, making the results of this study difficult to interpret, several remarks can be made regarding the results.

Although statistically insignificant due to large variances across participants, we have found two opposite trends in CBF as a function of time, mainly in the M1 and SMA ROIs, one relates to the pre scans, and the other to the post scans. The post scans that started at their maximal CBF level at the first day of learning, were found to have a lower value at the second time point, and even lower at the third time point, the last training day. Although increased in the retention session in the M1 and SMA, the CBF level did not return to its maximal value observed at the first day of training. The pre scans, on the other hand, started by low CBF values, increased significantly between the first and the second day, and retained their level in the retention day. This was not the case in the functionally-defined M1 ROI, where CBF decreases over time.

An intriguing aspect of this data is that while non-significant, the pre-training M1 and SMA CBF on all days except day 1 was found to be higher than the post-training CBF. This was especially the case in SMA ROI. A similar pattern was found across training days for M1, though the CBF differences were lower in this area.

These results are interesting in the light of previous fMRI learning results, where M1 tends to show decreased BOLD activation over time, while that of the SMA tends to show increases across days. While the CBF changes were very low and may not explain the fMRI data, it is possible that this task could increase blood at the earliest stage of the learning (day 1 was the only time point where CBF level in post scan exceeded the level in pre-scan), and decrease at advanced stages. The fact that CBF decreases between the pre and post scan might be attributed to an unknown bias, perhaps related to a difference In physiological state due to breathing rate changes during the task for example, which is counteracted in early training days by the effect of the training working to increase CBF. In later days, this effect becomes less and less significant as the subjects acquire higher

skill in performing the task. The time range of the possible task effect is unknown, since the ASL data were time-averaged. However, the fact that the ASL acquisition was performed immediately after the task supports the possibility that the observed trend was related to the task.

Except for the functionally-defined M1, when taking into account both pre and post scans, while statistically insignificant, an overall trend of increase CBF is observed. This indicates that learning may have a global effect on CBF, though this is likely partly masked by the high inter-subject variability. These considerations highlight the need for taking into account learning behavior when analyzing these results. In fact, the original study this is based on, showed a learning-related anatomical change, but this was only the case when correlating with behavior rather than day [47]. This is likely because there are several sub-groups of learners, with some subjects diluting the learning effect with a poor performance on the task.

However, if it is assumed that the day 0 versus day 5 difference is indicative of a learning effect which could be unveiled through more appropriate analyses of the data, the direction of the change over days is interesting. The CBF across days seems to increase across days (except for the functionally-defined M1), while some other studies have found that the M1 signal typically decreases across days [62]. An increased CBF could lead to a decreased BOLD signal through baseline effects. This is because the BOLD signal is a relative change from an unknown baseline. If this baseline is higher, than a similar hemodynamic change would lead to a smaller fractional change from baseline. It is therefore possible that previous studies showing a decreased BOLD across days are actually showing an increased BOLD baseline across days. Therefore, the interpretation that this decreased BOLD is due to a reduction of the importance of certain motor subareas in well-known tasks may be erroneous. The current study cannot unfortunately determine whether this is the case. However, a future study using this task and a calibrated fMRI framework could breakdown the BOLD signal into its component, including CBF, and determine whether this is the case.

5. Caveats

5.1 Registration

The neural activity, and therefore the expected areas of plasticity changes are located in a relatively well defined area in the motor cortex, namely, the finger area in the homunculus of the M1. Therefore, it is required that the anatomy of the motor cortex of each subject will be identified in the CBF maps. Thus, the accurate projection of the CBF on an anatomical image is necessary and can only be optimally achieved if the registration allows local deformations. In a linear registration with 12 DOF, the deformations can be done only globally, and thus not allowing customization, based on the individual difference in the brain structure.

In this study, the ASL data was registered to an anatomical space. However, for extracting the ROI, a template of the ROI had to be overlaid on the ROI in the anatomical space. Alternately, as was the case in this study, the CBF in the anatomical space can be registered to the same space of the ROI templates. Although the anatomical information can then serve for that purpose, it cannot be fully exploited using only linear operations. Future analyses could include non-linear deformations to improve the registration of the data to anatomical landmarks.

5.2 Lack of behavioural data

As mentioned previously, one of the greatest limitations of the current analyses is that they do not take into account the difference in behaviour between individuals. Another student also working on this data has done an analysis of the behavioural data and shown that there is a significant amount of variability in learning behaviour across subjects (personal communication). Since in previous use of this task this variability has been shown to be an important determinant of the ability to detect learning-related changes in MRI signals, it is possible that the current approach of quantifying learning across days is flawed. Future analyses of this data will use performance-related change in

CBF rather than daily comparison to assess the importance of vascular changes in the learning of this task.

5.3 ASL technique

As was discussed in the theoretical section, PASL is not the only technique that can be used to assess CBF in non-invasive MRI. The leading technique is pCASL, both in terms of SNR and reproducibility. This technique requires the flow of blood through a relatively thin slab of tagging in the neck area, and thus the existence of a special coil on top of a head coil for a 7T head-only machine such as the one used in this project. In the absence of a tagging coil, FAIR pulse sequence can be implemented using the head coil only. In this technique, outside of the imaging slab where no inversion pulse has affected the control image, the subtraction gives rise to extremely high intensity in the upper and lower parts of the image (see figure 4.1), as the tag image, in which the inversion pulse affects the entire brain, is subtracted from the control. These areas which are out of the imaging slab had to be removed, and consequently, part of the motor cortex was not included in the ROI.

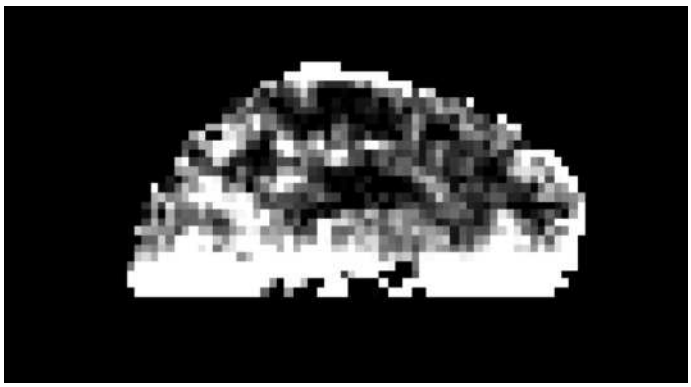

Figure 4.1. An image for demonstration the tagging artifact at upper and lower slices where the color scale is saturated.

Despite its advantages as a quantitative, physiologically-specific technique, ASL suffers from significant drawbacks. Large variability in CBF is often found among the different techniques, but also within a technique. As it is obtained from the subtraction of two similar images, it is by nature a low SNR technique. However, when implemented

well, ASL has been found to be reproducible and consistent with the nuclear medicine gold standards [85-86]. However, this is especially the case for pCASL sequence which include background suppression and multiple transit times. Moreover, in this specific case, although the QUIPSS methods make it unnecessary to estimate the bolus arrival time and the bolus duration, the assumption of uniform tagging is still needed. In other words, at any point in the imaging slab it is assumed that the same amount of tagged blood is entering. For example, it does not account the different transient times for different voxels, as is the case where the transit distance is longer. Certain imaging processing pipelines correct for that fact by applying slice timing correction. Future analyses of this data could include this approach.

6. Future work

Some areas of future improvements in terms of analysis possibilities have already been mentioned throughout the text. In summary, one of the main areas of improvement would be to implement a more robust registration to the common template using non-linear methods. Moreover, the template used to define the predefined ROI can be improved and combined the with functional localization. The improvement in predefining the ROI can be done by manual segmentation of brain areas after definition of areas functionally involved in the task using the functional localizer from day 0. The more distinct learning results shown for functionally-defined M1 show that in this task, precision is crucial, and thus this study can highly benefit from such a procedure. Other regions such as SMA should follow the same procedure and have a greater chance of showing learning-induced results as SMA is not as impacted as M1 from the loss of slices due to FAIR tagging issues (see paragraph one one the ASL technique section above). Additionally, inclusion of the behavioural data is likely to help tease out the learning effects. Future analyses of this data will include a linear regression of performance to identify learning-induced CBF changes.

Beyond the scope of this study, improvements in ASL implementation could be used to obtain more accurate and reliable learning-related CBF changes. Given the limitations of the 7T machine available for this study, a 3T implementation may be more likely to yield sufficient SNR since pCASL sequences are easier to implement on standard 3T machines. Furthermore, if the purpose is simply to measure resting CBF, a background-suppressed multi-delay pCASL sequence would be more likely to detect small CBF changes. Alternatively, a dual echo non-background suppressed single delay pCASL sequence with additional time points for further averaging could be used to perform a calibrated fMRI study of motor learning. Especially if the QUO_2 methods is used, this would allow to decompose the BOLD signal into its different baseline and reactivity components. This would permit a more nuanced understanding of the vascular and neural changes associated with motor learning.

This study also included additional data acquisitions which will, in the future, allow a better understanding of the learning process. During learning on each MRI acquisition day, the task was performed in the machine while vascular space occupancy (VASO) and BOLD data were acquired. VASO allows measurement of cerebral blood volume (CBV) change during a task. By combining the flow change before and after the task, with the BOLD and CBV change during the task, we may obtain a better understanding of the learning process involved in this task.

Beyond the scope of the mMPI project which this study was a part of, motor learning research can also benefit for combining electroencephalography (EEG), either separately or simultaneously to BOLD acquisition. EEG provides a direct measure of neural activity with high temporal resolution, thereby enables to characterize another aspect, a functional aspect, of the changes occurring during motor learning. Although the source localization in EEG consists a challenge, the combination of BOLD-EEG may provide complementary information regarding the source location.

Finally, as was discussed in the introduction, calibrated fMRI is another tool for addressing the investigation of plasticity induced changes in a quantitative way. Detecting changes in CBF can reveal only one aspect of neural plasticity. A next step might be

exploiting information regarding CBF in a motor learning related area and assessing $CMRO_2$. The ASL processing tool that were developed in this study can serve for research of that kind in the future.

7. Conclusions

The purpose of this study was to detect changes in CBF during and following a motor learning paradigm over 5 days. In most ROIs we have found a possible trends of increase CBF with learning. However, all comparisons between different time points were found to be non-significant. This is likely due to the low SNR of the ASL technique and the high variability both inter and intra-subject observed in our data. This variability may be lowered by improved processing and taking into account performance to account for individual learning rates. However, this study is intrinsically limited by the SNR of our FAIR approach, limited coil coverage, and short duration of the learning sessions. The learning session lasted only about 20 minutes, and thus it may be challenging to detect changes associated with this paradigm, especially when using a low SNR technique was large. Despite the low intensity of the learning activity, changes were detected in the previous studies, providing a motivation to explore those changes more quantitatively. However, the current work provides a tool, namely, an ASL data processing pipeline, as well as practical suggestions regarding a possible continuation in the search for characterizing the vascular aspect of motor learning.

References

[1] Kolb, B. (2013). Brain Plasticity and Behavior. *American physiological society*. 12(1), 1-5

[2] Jeans, A. and Erisi M. (2008). Brain Histology. *Practical Neurology*. 8, 303-310

[3] Marblestone, A.H. (2013). Physical Principles for Scalable Neural Recording. *Frontiers in Computational Neuroscience*. doi: 10.3389/fncom.2013.00137

[4] Van Praag, H. (1999). Running Enhances Neurogenesis, Learning, and Long-term Potentiation in Mice. *PNAS*. 96(23), 13427-13431

[5] Fordyce, D.E. and Wehner, J.M. (1993). Physical Activity Enhances Spatial Learning Performances with an Associated Alternation in the Hippocampal Protein Kinase C Activity in C57BL/6 and DBA/2 Mice. *Brain Research*. 619, 111-119

[6] Anderson, B.J. (2000). Exercise Influences Spatial Learning in the Radial Arm Maze. *Physiology & behavior*. 70, 425-429

[7] Vaynman, S. (2004). Hippocampal BDNF mediates the Efficacy of Exercise on Synaptic Plasticity. *European Journal of Neuroscience*. 20, 2580-2590

[8] Kerr, A.L. (2010). Angiogenesis but not Neurogenesis is Critical for Normal Learning and Memory Acquisition. *Neuroscience*. 171, 214-226

[9] Zhang, P. (2013). Early Exercise Improves Cerebral Blood Flow through Increased Angiogenesis in Experimental Stroke Rat Model. *Journal of Neuroengineering and rehabilitation*. 10(43), 1-10

[10] Swain, R.A. (2003). Prolonged Exercise Induces Angiogenesis and Increases Cerebral Blood Volume in Primary Motor Cortex of the Rat. *Neuroscience*. 117, 1037-1046

[11] Girouard, H. and Iadecola C. (2006). Neurovascular coupling in the normal brain and in hypertension, stroke and Alzheimer disease. *Journal of Applied Physiology*. 100, 328-335

[12] Gauthier, C.J. (2015). Hearts and Minds: Linking Vascular Rigidity and Aerobic Fitness with Cognitive Aging. *Neurobiology of Aging*. 36, 304-314

[13] Petersen, T.H. (2012). The Motor Cortex Drives the Muscles during Walking in Human Subjects. *The Journal of Physiology*. DOI: 10.1113/jphysiol.2012.227397

[14] Armstrong, D.M. (1988). The Supraspinal Control of Mammalian Locomotion. *Journal of Physiology*. 405, 1-37

[15] Black, J.E. (1990). Learning Causes Synaptogenesis, Where Motor Activity Causes Angiogenesis, in Cerebellar Cortex of Adult Rays. *Neurobiology*. 87, 5568-5572

[16] Gilbert, P.F. (1977). Purkinje Cell Activity during Motor Learning. *Brain Research*. 128, 309-328

[17] Tabatabaei-Jafari, H. (2015). Cerebral Atrophy in Mild Cognitive Impairment: A Systematic Review with meta-Analysis. *Alzheimer's and Dementia*. 1(4), 487-504

[18] Raz, N. (1999). Aging of the Brain and its Impact on Cognitive Performance: Integration of Structural and Functional Findings. *Aging of the brain*. Chapter 1

[19] Cabeza, R. (2002). Aging Gracefully: Compensory Brain Activity in High-Performing Older Adults. *Neuroimage*. 17, 1394-1402 doi:10.1006/nimg.2002.1280

[20] D'Esposito, M. (2003). Alternations in the BOLD fMRI Signal with Ageing and Disease: a Challenging for Neuroimaging. *Nature Review*. 4, 863-872 doi:10.1038/nrn1246

[21] Meltzer, C.C. (2000). Does Cerebral Blood Flow Decline in Healthy Aging? A PET Study with Partial-Volume Correction. *The Journal of Nuclear Medicine*. 41, 1842-1848

[22] Kastrup, A. Changes of Cerebrovascular C02 Reactivity during Normal Aging. *Stroke*. 29, 1311-1314 https://doi.org/10.1161/01.STR.29.7.1311

[23] Leoni, R.F. (2017). Cerebral Blood Flow and Vascoreactivity in Aging: an Arterial Spin Labeling Study. *Brazilian Journal of Medical and Biological Research*. doi: 10.1590/1414-431X20175670

[24] Middleton, L.E. (2008). Changes in Cognition and Mortality in Relation to Exercise in Late Life: a Population Based Study. doi:10.1371/journal.pone.0003124

[25] Cox. E.P. (2016). Relationship between physical activity and cognitive function in apparently healthy young to middle-aged adults: A systematic review. *Journal of Science and Medicine in Sport*. 19, 616-628

[26] Bherer, L. (2014). A Review of the Effects of Physical Activity and Exercise on Cognitive and Brain Functions in Older Adults. *Journal of Aging Research*. doi: 10.1155/2013/657508

[27] Bergmann, O. (2015). Adults Neurogenesis in Humans. *Cold Spring Harbor Perspective in Biology*. doi: 10.1101/cshperspect.a018994

[28] Vaupel P. (1989). Blood flow, oxygen and nutrient supply, and microenvironment of human tumors: a review. *Cancer Research*. 49, 6449-6465

[29] Brown A.D. (2010). Effects of Cardiorespiratory Fitness and Cerebral Blood Flow on Cognitive Outcome in Older Woman. *Neurobiology of Aging*. 31, 2047-2057

[30] Sweatt, J.D. (2004). Hippocampal Function in Cognition. *Psychopharmacology*. 174, 99-110 doi 10.1007/s00213-004-1795-9

[31] Maass, A. (2014). Vascular hippocampal plasticity after aerobic exercise in older adults. *Molecular Psychiatry*. doi:10.1038/mp.2014.114

[32] Park, D.C. (2009). The adaptive brain: aging and neurocognitive scaffolding. *Annual Review in Psychology*. 60, 173-196 doi 10.1146/annurev.psych.59.103006.093656

[33] Davis, T.L. (1998). Calibrated functional MRI: mapping the dynamics of oxidative metabolism. *The National Academy of Sciences*. 95, 1834-1839

[34] Chiarelli, P.A. (2007) A calibrated method for quantitative BOLD fMRI based on hyperoxia. *NeuroImage*. 37, 808-820

[35] Gauthier, C.J. (2013). A generalized procedure for calibrated MRI incorporating hyperoxia and hypercapnia. *Human Brain Mapping*. 34, 1053-1069

[36] Gauthier, C.J. (2011). Magnetic resonance imaging of resting OEF and CMRO2 using a generalized calibration model for hypercapnia and hyperoxia. *NeuroImage*. 60, 1212-1225

[37] Gauthier, C.J. (2012). Age dependence of hemodynamic response characteristics in human functional magnetic resonance imaging. *Neurobiology of Aging*. 34, 1469-1485

[38] Chiarelli, P.A. (2007). Sources of systematic bias in hypercapnia-calibrated functional MRI estimation of oxygen metabolism. *NeuroImage*. 34, 35-43

[39] Chen, J.J. (2009). BOLD-specific cerebral blood volume and blood flow changes during

neuronal activation in humans. *NMR in Biomedicine*. 22, 1054-1062 DOI:10.1002/nbm.1411

[40] Bruce, F. (2000). Measuring the thickness of the human cerebral cortex from magnetic resonance images. *PNAS*. 97(20), 11050-11055

[41] Gagnon, L. (2016). Validation and optimization of hypercapnic-calibrated fMRI from oxygen-sensitive two-photon microscopy. *Philosophical transections B*. http://dx.doi.org/10.1098/rstb.2015.0359

[42] Wang, Y. and Liu, T. (2014). Quantitative susceptibility mapping (QSM): decoding MRI data for a tissue magnetic biomarker. *Magnetic Resonance in Medicine*. 73(1), 82-109.

[43] Bammer, R. (2003). Basic principles of diffusion-weighted imaging. *European Journal of Radiology*. 45, 169-184

[44] Mukherjee, P. (2008). Diffusion tensor MR imaging and fiber tractography: theoretic underpinnings. *American Journal of Neuroradiology*. 29(4), 632-641

[45] Marques J. P. (2010). MP2RAGE, a self bias-field corrected sequence for improving segmentation and T1-mapping at high field. *NeuroImaging*.

[46] Martijn, P. H. (2010). Exploring the brain newtwork: a review on resting-state fMRI functional connectivity. *European Neuropsychopharmacology*. 20, 519-534

[47] Gryga, M. (2012). Bidirectional gray matter changes after complex motor skill learning. *Frontiers in Systems Neuroscience*. doi: 10.3389/fnsys.2012.00037

[48] Kandel, R. K. (2013). Principles of neural science, fifth edition. Chapter 22, 475-497

[49] Cheyne D. (1990). Homuncular organization of human motor cortex as indicated by neuromagnetic recordings. *Neuroscience Letters*. 122, 17-20.

[50] Maguire E. A. (2006). London taxi driver : a structural MRI and Neuropsychological analysis. *Hippocampus*. 16, 1091-1101.

[51] Gaser, C. (2003). Brain structure differ between musicians and non-musicians. *The Journal of Neuroscience*. 23(27), 9240-9245.

[52] Rizzolatti, G. (2001). The cortical motor system. *Neuron*. 31, 889-901.

[53] Kandel, R. K. (2013). Principles of neural science, fifth edition. Chapter 37, 835-864.

[54] Nudo, R. J. (1996). Use-dependent alternations of movement representations in primary motor cortex of adult squirrel monkeys. *The Journal of Neuroscience*. 16(2), 785-807.

[55] Kleim, J. A. (1998). Functional reorganization of the rat motor cortex following motor skill learning. *Journal of Neurophysiology*. 80, 3321-3325.

[56] Classen, J. (1998). Rapid plasticity of the human cortical movement representation induced by practice. *Journal of Neurobiology*. 79(2), 1117-1123.

[57] Kleim, J. A. (2004). Cortical synaptogenesis and motor map reorganization occur during late, but not early, phase of motor skill learning. *The Journal of Neuroscience*. 24(3), 628-633.

[58] Alexander G. E. (1986). Parallel organization of functionally segregated circuits linking basal ganglia and cortex. *Annual Review of Neuroscience*. 9, 357-381.

[59] Kandel, R. K. (2013). Principles of neural science, fifth edition. Chapter 42, 960-981

[60] Houk, J. C. (1995). Distributed modular architectures linking basal ganglia, cerebellum and cerebral cortex: their role in planning and controlling action. *Cerebral Cortex*. 2, 95-110.

[61] Steele, C. J. (2010). Specific increases within global decreases: a functional magnetic resonance imaging investigation of five days of motor sequence learning. *The Journal of Neuroscience*. 30(24), 8332-8341.

[62] Penhune, V. B. (2011). Parallel contributions of cerebellar, striatal and M1 mechanisms to motor sequence learning. *Behavioural Brain Research*. 226, 579-591

[63] Tardif, C.L. (2017). Investigation of the confounding effects of vasculature and metabolism on computational anatomy studies. *Neuroimage*. 1(149), 233-243. doi: 10.1016/j.neuroimage.2017.01.025

[64] Chapman, S.B. (2013). Neural Mechanisms of Brain Plasticity with Complex Cognitive Training in Healthy Seniors. *Cerebral Cortex*. doi:10.1093/cercor/bht234

[65] Abragam, A. (1961). Principles of nuclear magnetism. *Oxford Science Publication*.

[66] Slichter, C.P. (1990). Principles of Magnetic resonance – third enlarged and updated edition. *Sprinter*.

[67] Nishimura, G.N. (2010). Principles of magnetic resonance imaging. *Stanford University*.

[68] Huettel S.A. (2014). Functional magnetic resonance imaging – third edtion. *Sinauer*

[69] Cuenod C.A. and Balvay D. (2013). Perfusion and vascular permeability: Basic concepts and measurement in DCE-CT and DCE-MRI. *Diagnostic and Interventional Imaging*. 94, 1187-1204

[70] Bokkers, R.P.H. (2010). Arterial spin labeling perfusion MRI at multiple delay times: a correlative study with H2 15O positron emission tomography in patients with symptomatic carotid artery occlusion. *Jouranl of Cerebral Blood Floow and Metabolism*. 30, 222-229

[71] Federau, C. (2015). Functional Mapping of the Human Visual Cortex with Intravoxel Incoherent Motion MRI. doi:10.1371/journal.pone.0117706

[72] Dai, W. (2008). Continuous Flow Driven Inversion for Arterial Spin Labeling Using Pulsed Radiofrequency and Gradient Fields. *Magnetic Resonance in Medicine*. 60(6), 1488-1497

[73] Wong E.C. (1997). Implementation of Quantitative Perfusion Imaging Techniques for Functional Brain Mapping using Pulsed Arterial Spin Labeling. *NMR in Biomedicine*. 10, 237-249

[74] Buxton R.B. (1998). A General Kinetic Model for Quantitative Perhsion Imaging with Arterial Spin Labeling. *Magnetic Resonance in Medicine*. 40, 383-396

[75] Frank, Q.Y. (1996). Perfusion Imaging of the Human Brain at 1.5 T Using a Single-Shot EPI Spin Tagging Approach. *Magnetic Resonance in Medicine*. 36, 219-224

[76] Stanisz, G.J. (2005). T1, T2 Relaxation and Magnetization Transfer in Tissue at 3T. *Magnetic Resonance in Medicine*. 54, 507–512

[77] Johnston, M.E. (2015). Multi-TI Arterial Spin Labeling MRI with Variable TR and Bolus Duration for Cerebral Blood Flow and Arterial Transit Time Mapping. *IEEE TRANSACTIONS ON MEDICAL IMAGING*. 1392-1402

[78] Buxton, E.C. (1998). Quantitative Imaging of Perhsion Using a Single Subtraction (QUIPSS and QUIPSS 11). *Magnetic Resonance in Medicine*. 39, 702-708

[79] Liu, T.T. (2004). A signal processing model for arterial spin labeling functional MRI. *NeuroImage*. 24, 207– 215

[80] Kang, H.R. (2006). Computationnel color technology. T*he Society of Photo-optical Instrumentation Engineers*

[81] Triantafyllou, C. (2005). Comparison of physiological noise at 1.5 T, 3 T and 7 T and optimization of fMRI acquisition parameters. *NeuroImage*. 26, 243– 250

[82] Krüger, G. and Glover, G.H. (2001). Physiological Noise in Oxygenation-Sensitive Magnetic Resonance Imaging. *Magnetic Resonance in Medicine*. 46,631–637

[83] Cavusoglu, M. (2009). Comparison of pulsed arterial spin labeling encoding schemes and absolute perfusion quantification. *Magnetic Resonance Imaging*. 27, 1039-1045

[84] *Jenkinson, M., Bannister, P., Brady, J. M. and Smith, S. M. Improved Optimisation for the Robust and Accurate Linear Registration and Motion Correction of Brain Images. NeuroImage, 17(2), 825-841, 2002*

[85] Fan, A.P. (2017). Long-Delay Arterial Spin Labeling Provides More Accurate Cerebral Blood Flow Measurements in Moyamoya Patients. *Stroke*. https://doi.org/10.1161/STROKEAHA.117.017773

[86] Chen, Y. (2011). Test–Retest Reliability of Arterial Spin Labeling With Common Labeling Strategies. Journal of Magnetic Resinance Imaging. 33, 940–949

[87] Woolrich, M.W. (2009). Bayesian analysis of neuroimaging data in FSL. *NeuroImage*, 45:S173-86, 2009